THE EFFECT OF DEEP ROLLING PROCESS PARAMETERS ON SUBSURFACE HARDNESS DISTRIBUTION IN DEEP ROLLING OF EN AW6061 ALUMINIUM ALLOYS

EN AW6061 ALÜMİNYUM ALAŞIMLARINDA DERİN OVALAMA PROSES PARAMETRELERİNİN YÜZEY ALTI SERTLİK DAĞILIMINA ETKİSİ

MUHAMMET AYKUT ÖZDEMİR

ASST. PROF. DR. MEHMET OKAN GÖRTAN
Supervisor

Submitted to
Graduate School of Science and Engineering of Hacettepe University
as a Fulfilment to the Requirements
for the Award of the Degree of Master of Science
in Mechanical Engineering.

2020

ÖZET

EN AW6061 ALÜMİNYUM ALAŞIMLARINDA DERİN OVALAMA PROSES PARAMETRELERİNİN YÜZEY ALTI SERTLİK DAĞILIMINA ETKİSİ

Muhammet Aykut ÖZDEMİR

Yüksek Lisans, Makina Mühendisliği Bölümü
Tez Danışmanı: Dr. Öğr. Üyesi Mehmet Okan GÖRTAN
Mayıs 2020, 40 sayfa

Alüminyum ve alüminyum alaşımları, mekanik dayanım ve elektrik iletkenliği özelliklerinden dolayı iletken yapımında sıkça kullanılan malzemelerdir. Bakırla karşılaştırıldığında, hafif ve ucuz olması sebebiyle iletken kullanımının yoğun olduğu alanlarda avantaj sağlamaktadır. Fakat, elektrik iletkenliğinin bakıra göre düşük oluşu elektrik iletiminde kayıplara sebep olmaktadır. Bu nedenle, alüminyum ve alüminyum alaşımları kullanılarak hem yüksek dayanıma sahip hem de yüksek iletkenlik gösteren iletken elde edilmesi her zaman önemli bir konu olmuş ve birçok çalışmada yer almıştır.

Son yıllarda yapılan çalışmalar, uygun ısıl işlemlerin yardımıyla, ince tanecik yapılı alaşımların yüksek dayanıma ve yüksek iletkenliğe bir arada sahip olabileceğini göstermektedir. İnce tanecik yapılı alaşım elde etmek için birçok farklı aşırı plastik deformasyon yöntemi kullanılmaktadır. Fakat, ilgili aşırı plastik deformasyon yöntemleri henüz yeterince ticarileşememiş ve sürekli üretime adapte edilememiş olup aynı zamanda yüksek maliyetlidirler. Öte yandan, derin ovalama yıllardır kullanılan bir yöntem olup parça yüzeyinde ve yüzey altı bölgelerinde plastik deformasyonla mikro-yapıyı değiştirebilen bir yöntemdir. Ayrıca, derin ovalama düşük takım ve işletme maliyetlerine sahiptir ve sürekli üretime uygun hale getirilebilir bir yöntemdir. Bahsedilen özellikleri

sayesinde derin ovalama, ilgili iletkenlerin üretiminde kullanılmaya elverişli olabilir. Bu sebeple, derin ovalama proses parametrelerinin alüminyum alaşımlarının belirli özelliklerini nasıl etkilediğini anlamak amacıyla böyle bir çalışma gerçekleştirilmiştir.

Bu çalışmada, farklı temper durumlarındaki EN AW6061 alüminyum alaşımlarında derin ovalama kuvvetinin, parça yüzey ve yüzey altı bölgelerindeki pekleşmeye ve yüzey pürüzlülüğüne etkisi incelenmiştir. Çalışma, sayısal ve deneysel çalışmalar olmak üzere iki bölümde gerçekleştirilmiştir. Elde edilen bulgular sonucu, T4 temper durumundaki malzemede %60'a varan oranlarda sertlik artışı elde edilmiş ve yüksek kuvvetlerde yüzeyden 2 mm daha derindeki katmanlarda dahi sertliğin arttığı görülmüştür. Öte yandan, T6 temper durumundaki malzemede yalnızca en yüksek kuvvette sertlik artışı elde edilmiş ve 0.1 mm'den daha derin katmanlarda sertlik artışı gerçekleşmemiştir. Son olarak, sertlik dağılımı ve yüzey pürüzlülüğü sonuçları sayısal çalışmalardan elde edilen öngörüler ile birlikte değerlendirilerek tartışılmıştır.

Anahtar kelimeler: Derin ovalama, aşırı plastik deformasyon, sertlik dağılımı, alüminyum iletkenler, ince taneli alaşımlar.

ABSTRACT

THE EFFECT OF DEEP ROLLING PROCESS PARAMETERS ON SUBSURFACE HARDNESS DISTRIBUTION IN DEEP ROLLING OF EN AW6061 ALUMINIUM ALLOYS

Muhammet Aykut ÖZDEMİR

Master of Science, Department of Mechanical Engineering
Supervisor: Asst. Prof. Dr. Mehmet Okan GÖRTAN
May 2020, 40 pages

Aluminium and aluminium alloys are widely used in production of electrical conductors, owing to their mechanical strength and electrical conductivity properties. Also, aluminium is cheaper and lighter than copper. Thus, it is advantageous to use aluminium conductors in areas where high volumes of conductors are used. However, its electrical conductivity is lower than copper and this causes losses in transmission of electricity. Therefore, producing conductors that have both high mechanical strength and high electrical conductivity has always been an important topic and took place in many studies.

In recent studies, it is shown that together with appropriate heat-treatments ultra-fine-grained alloys can reveal high strength and high conductivity together. In order to obtain ultra-fine-grained alloys, many different severe plastic deformation methods can be used. However, these methods are not suitable for continuous production lines and not yet commercialized and yield high costs. On the other hand, deep rolling is a method used for years, that can alter the microstructure at the surface and subsurface area of a component by plastic deformation. In addition, it has low tooling and operating costs and can be modified to suit in continuous production lines. Because of these features, deep rolling can be convenient to be used in production of such conductors. Therefore, such a

study was carried out to understand how parameters of deep rolling effect certain properties of an aluminium alloy.

In this study, the effect of deep rolling force on work-hardening state and surface roughness at the surface and subsurface area of a component made of differently tempered EN AW6061 aluminium alloy is investigated. The study was carried out in two parts which are experimental work and numerical simulation part. According to the results, high forces provided increase in hardness values at layers deeper than 2 mm for T4 tempered material. Also, increase in hardness values can go up to 60% for T4 tempered material. However, for T6 tempered material, increase in hardness values was obtained only at highest rolling force and no hardness increase was observed at layers deeper than 0.1 mm. In conclusion, the predictions obtained from numerical simulations, hardness distributions and surface roughness results were evaluated and discussed together.

Keywords: Deep rolling, severe plastic deformation, hardness distribution, aluminium conductors, ultra-fine-grained alloys.

ACKNOWLEDGEMENTS

Firstly, I would like to express my appreciations and respects to my supervisor, Asst. Prof. Dr.-Ing. Mehmet Okan Görtan, for his precious efforts, guidance and assistance.

I would like to thank to TÜBİTAK SAGE, that is one of the most eligible institutions of this country, for the supports and facilities that helped me a lot in this study.

I also would like to thank to my former employer, Volkan Aydınol, for his encouragement and support during my first years of work life and postgraduate study.

I especially would like to thank to dear Didem Akyol for her patience, kindness and great support.

I would like to express my deepest gratitude to my lovely family for their great supports and encouragements during my entire life.

Muhammet Aykut Özdemir
May 2020, Ankara

TABLE OF CONTENTS

LIST OF FIGURES

LIST OF TABLES

SYMBOLS AND ABBREVIATIONS

Symbols

Ra	Arithmetical mean deviation of the assessed roughness profile
Rq	Root mean square deviation of the assessed roughness profile
Rz	Maximum height of the roughness profile
σ	Stress
σ_{UTS}	Tensile strength
σ_Y	Yield strength
$\sigma_{\max}$	Maximum principal stress
$\overline{\sigma}$	Effective von-Mises stress
ϵ	Strain
ϵ_0	Initial strain
$\dot{\bar{\epsilon}}$	Effective plastic strain rate
C	Critical material constant
K	Material constant
n	Material constant
e	Euler' number

Abbreviations

ARB	Accumulative Roll Bonding
ASTM	American Society for Testing and Materials
AW	Wrought product
CG	Coarse-grained
CNC	Computer Numerical Control
DR	Deep Rolling
EN	Euronorm
ECAP	Equal Channel Angular Pressing
ECAP-PC	Equal Channel Angular Pressing-Parallel Channels
FSP	Friction Stir Processing
HE	Hydrostatic Extrusion

HPT	High Pressure Torsion
IACS	International Annealed Copper Standard
MEMS	Microelectromechanical Systems
SI	Système International
SPD	Severe Plastic Deformation
TE	Twist Extrusion
TEPS	Total Equivalent Plastic Strain
UFG	Ultra-fine grain

1. INTRODUCTION

Aluminium has a high electrical conductivity, such that pure aluminium shows 61% IACS (International Annealed Copper Standard). Aluminium is in the second rank after copper in terms of electrical conductivity [1]. Compared to copper, aluminium is lighter, cheaper and the ratio of electrical conductivity to weight is twice that of coppers. Also, aluminium has a high ratio of mechanical strength to weight and moreover there are numerous ways to increase its mechanical strength such as cold work.

The advantages of aluminium as a conductor compared to copper introduced its usage as a conductor material and it has a trending use in overhead power lines starting from the end of the 19^{th} century [1]. This situation increased the need for utilization of the aluminium conductors in order to attain conductors that have both high mechanical strength and high electrical conductivity. There are classical processes, such as alloying, tempering and cold work, used for decades to improve aluminium's mechanical strength. However, electrical conductivity of such processed material is usually decreased. In order to overcome this problem, microstructural modifications by severe plastic deformation (SPD) and heat treatment methods to create ultra-fine-grained alloys are addressed by researchers [2].

There are numerous SPD methods, but majority of these methods yield high costs and not yet commercialized. However, a well-known surface treatment method, deep rolling (DR), is used for years to create plastic deformation on surface and subsurface of the components. Also, DR is an effective method to alter microstructure at near surface area and can increase mechanical and fatigue strength of components [3, 4]. Moreover, with the right modifications, DR can be suited in continuous production of differently shaped components [3]. Therefore, DR holds a potential to be used in production of such conductors.

In this study, the influence of rolling force, which is the most important parameter, on component's state of work-hardening at near surface area and on surface properties was investigated. The study was carried out in two parts such that, application of DR to components followed by hardness and surface roughness measurements was conducted

in experimental part of the study. Besides, in finite element analysis part, DR application was simulated to anticipate parameter effects. In addition, the work material was chosen to be EN AW6061 aluminium alloy in T4 and T6 temper conditions which is widely used in industry.

It is observed that, near surface properties of T4 and T6 tempered materials show dramatically different behaviours than each other after subjecting to DR at different forces. That is, T4 tempered material showed high ratios of hardness rise that goes up to layers even deeper than 2 mm. On the other hand, hardness increase was only obtained for specimen rolled at highest force for T6 tempered material and the rise was not observed at layers deeper than 0.1 mm. Besides, force increase provided deeper hardened layers for T4 tempered material. The alteration of hardness distributions and surface roughness values was evaluated together with predictions obtained from numerical simulations and discussed briefly.

2. STATE OF THE ART

2.1. Electrical Conductivity, Conductors

There are many materials that are used as conductors. However, copper and aluminium deserves special interest since they are the most used conductors [5]. Compared to copper, aluminium is lighter and cheaper. In terms of conductivity per unit weight, aluminium doubles the copper and the ratio of mechanical strength to weight is also higher than copper [1, 6]. Therefore, aluminium wire and bus conductors were started to be employed in overhead power lines since the end of the 19^{th} century and today, aluminium and its alloys are used pretty much in overhead power lines [1, 7].

For functional purposes, high strength, high conductivity, corrosion resistance and a good combination of these properties are expected from the conductors [1, 8, 9]. Commercially pure aluminium is quite conductive, but it has relatively low strength values and thus its mechanical strength is increased by alloying, by tempering and by cold work. However, these processes usually cause Al's conductivity to decrease dramatically [10-12].

Conductivity and mechanical strength of conductor materials are very sensitive to the microstructure [8, 13]. Conventional processes cannot provide further improvements on conductivity and strength of conductor materials simultaneously [13, 14]. However, it is possible to increase mechanical strength and electrical conductivity simultaneously by appropriate microstructural modifications [8].

Studies in recent period shows that, with appropriate heat treatments, ultra-fine grained (UFG) alloys obtained by severe plastic deformation methods can show high strength and high conductivity together. For instance, a good combination of strength and conductivity was obtained by high pressure torsion (HPT) followed by artificial aging (AA) of EN AW6101 alloy [10]. Moreover, in another study, by HPT at 180 °C, tensile strength of EN AW6060 alloy was increased about 40% while its conductivity was increased about 8% compared to standard T6 tempering [15]. Also, in the same study, by equal-channel angular pressing with parallel channels (ECAP-PC) followed by AA, tensile strength of EN AW6063 alloy was increased about 50% while its conductivity was increased about 7% compared to T6 tempering [15].

2.2. UFG Alloys

UFG materials can be defined as materials those have grain sizes smaller than 1 μm. Generally, UFG materials are obtained by SPD methods such as equal-channel angular pressing (ECAP), high pressure torsion (HPT), accumulative roll bonding (ARB), hydrostatic extrusion (HE), twist extrusion (TE) and friction stir processing (FSP). There are many application areas that may benefit from UFG materials like dental implants, electrical conductors, micro devices, microelectromechanical systems (MEMS) and nano magnets [16]. Thus, in recent era, studies on UFG creation by SPD methods and the effect of SPD on mechanical properties were increased notably and additionally promising outcomes were attained from these studies [16-18].

A study shows that, UFG creation by SPD can enhance mechanical properties of age-hardenable Al alloys considerably [17]. Also, in different studies, UFG materials obtained by SPD methods reveal higher strength values compared to their coarse-grained (CG) variants [16, 19]. Moreover, even though in conventional methods, ductility is affected conversely by mechanical strength, it is possible for UFG materials to have both high strength and good ductility properties [16, 20, 21].

Commercialization and spread of the applications of UFG materials present potential benefits. The enhancement in material properties and obtaining state of the art products from UFG materials are possible [16]. Nevertheless, UFG materials are not commercialized and are not widespread. Because, there are still challenges to be overcame such as reducing costs and lower the wastage [16]. Thus, to be cost effective, endurable processes and robust SPD tools should be developed and also production techniques should allow continuous and multiple shaped production [17].

2.3. Deep Rolling

Deep rolling is a mechanical surface treatment method that can create plastic deformation on the surface and subsurface area of the exposed component. The process is done by applying a predetermined force on the outer surface of a component by a tool with balls or a roller. Tool type can be selected upon the geometry of the component that will be rolled. In addition, these tools can suit to a lathe’s chuck or a milling machine’s tool holder. So, differently shaped components can be rolled without investing so much in

tooling. The applied force can be either generated hydraulically or mechanically. An illustration that shows DR process can be seen in Figure 2-1. DR process is performed under the parameters that can be counted as; rolling force (or pressure), number of runs, rolling diameter, feed speed and friction coefficient.

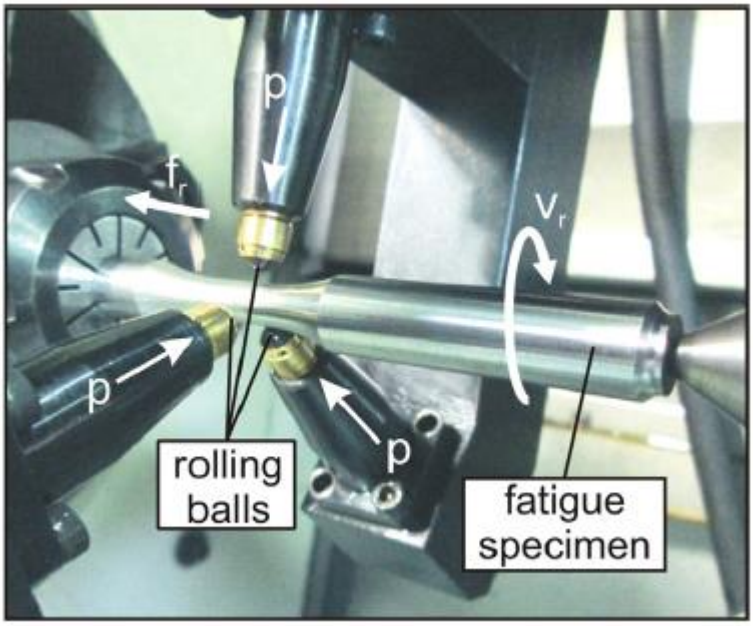

Figure 2-1: An example of deep rolling setup [22].

DR is mostly used to increase fatigue strength of metallic materials those subjected to cyclic loading [3, 4]. This enhancement by DR is accomplished via altering a material's state of residual stress, work hardening, and surface roughness in surface and subsurface area. Besides, it is known for years that DR can produce compressive residual stress and can provide work hardening on the exposed area of a metallic material [3, 4]. Additionally, it can also decrease surface roughness and can create a shiny surface [3, 4]. These abilities make DR a widely used surface treatment method in areas such as; crankshafts, surgical implants, turbine blades of power plants and some components in aerospace industry [3]. Also, common materials subjected to DR can be given as; titanium alloys, carbon steels, stainless steels and aluminium alloys [4].

The fatigue life of metallic components is mainly influenced by states of work hardening, compressive residual stress and surface roughness. The effects of these characteristics on fatigue behaviour is given in Figure 2-2. DR can help to improve fatigue life of components in two way; first, increases surface hardness by work hardening and thus

prevents crack initiation and second, creates compressive residual stress and thus prevents propagation of existing cracks [4, 23]. In general, DR creates a smooth surface with low surface roughness, because of these components mainly fails due to crack initiation and it is more important to obtain adequate strain hardening for deep rolled components [3].

Table 1

	Crack nucleation	Crack propagation
Surface roughness	Accelerates	No effect
Cold work	Retards	Accelerates
Residual compressive stress	Minor or no effect	Retards

Figure 2-2: Effect of surface characteristics on fatigue process [23].

There are many studies regarding the effect of DR on surface characteristics and fatigue life of components. These investigations can be summarized as; combination of heat treatments and DR, fatigue life alterations of deep rolled components at elevated temperatures, optimizing process parameters and understanding their effects by experiments as well as numerical simulations and microstructural alterations.

Early studies stated that, titanium alloy and aluminium alloy specimens reveals significant fatigue life increase when subjected to DR treatment [23]. Recent and early studies show that the beneficial effects of DR, i.e. compressive residual stresses, strain hardening, low surface roughness, improves fatigue life of components made of carbon steels, stainless steels, aluminium and titanium alloys for normal cyclic loadings [24-26]. However, cycling loading of components at high temperatures or at high stress amplitudes generally vanishes the beneficial effects and makes DR ineffective for fatigue life at these conditions [24-26]. Regarding combination of heat treatments with DR, it can be said that, an optimized heat treatment sequence prior to DR treatment usually gives the best outcomes on fatigue life for aluminium alloys [27, 28]. Moreover, deep rolled components are found to be more resistant to fretting fatigue, corrosion and corrosion fatigue and also foreign object damage which are pronounced effects usually in aerospace applications [3, 29].

Another aspect is to investigate how process parameters influence DR outcomes. The most effective and important parameter is the rolling pressure. It is critical to apply sufficient pressure on the component to obtain plastic deformation but then applying higher pressures may even affect DR outcomes inversely [4, 30]. It can be said that, increase in rolling pressure and number of passes increases effected depth and causes higher surface hardness on the components [31]. In addition, residual stresses convert from tensile to compressive but after exceeding a certain pressure no further increase can be obtained in compressive residual stresses [31]. Besides, surface roughness decreases at low rolling pressures but high pressures may have detrimental effects on surface roughness and may even lead to spalling at the surface [31]. Tensile strength of the materials was found to be increased with high rolling pressures but yield strength was effected conversely [22, 31]. It is also stated that, high surface hardness prior to DR decreases its effect on hardness increase [22]. In addition to all that, process parameters are crucial factors and need to be optimized. Therefore numerical simulations can be used to determine optimal process parameters prior to real study and can help to save time and money as well [4, 29].

The alteration of microstructure at the surface and near surface area is also an important outcome. Recent studies reveal that DR is an effective method to alter the microstructure and may induce many different types of microstructure, including nanocrystals, depending on process parameters and materials subjected [3, 4]. It is reported that DR can lead to creation of nanocrystalline and highly strain hardened layers at the surface-subsurface areas for titanium alloys and stainless steels [32, 33]. DR can increase dislocation density and lead increase in hardness values at component's surface [31]. There are also relatively new methods of this treatment to alter microstructure and other properties exist and still in development such as DR at high or low temperatures [4, 34, 35].

Briefly, it can be said that, DR is a cost-effective, less time-consuming surface treatment method to alter residual stress state, work hardening state, surface roughness along with microstructure state of many different metallic materials and it offers a promising future.

3. MOTIVATION AND METHODOLOGY

3.1. Motivation

Aluminium and aluminium alloys are widely used as conductor material. In recent years, numerous studies were carried out to increase aluminium's strength while preserving its high conductivity. These studies show that UFG Al alloys can demonstrate both high electrical conductivity and high strength at the same time. There are many methods to obtain an UFG Al alloy via SPD. However, one of the main challenges with SPD techniques is developing high volume and continuous processing equipment. This is the point where DR methods can be used effectively. DR method can be modified in order to suit high volume and continuous processing of materials. The motivation behind this study is that if SPD is achievable on Al alloys with DR, one can attain UFG Al alloys that have increased strength with preserved conductivity and the way to produce such conductors in high volumes can be opened. As an early step about this subject, the present study was carried out.

3.2. Methodology

The experimental study started with receiving EN AW6061 grade round aluminium bars that are in non-tempered condition. These bars were divided into ten equal pieces and were separated in two groups each containing five pieces. First group of pieces were heat-treated to T4 temper condition and second group of pieces were heat-treated to T6 temper condition. The heat-treating sequence of T4 and T6 conditions were given in Table 3-1.

Table 3-1: Heat-treating sequence for T4 and T6 conditions.

T4	T6
500 °C, 2 hrs	500 °C, 2 hrs
Quenched	Quenched
Room temperature, 4 days	200 °C, 2.5 hrs
-	Room temperature

After tempering, the bars were lightly machined to 15 mm outside diameter using turning. Consequently, there were two groups of parts which are machined and are in two different temper condition. Then, two specimens from each group selected to perform tensile tests to determine the strengths of the tempered materials. Tensile tests were performed on a Servo Hydraulic Tensile Testing Equipment and specimens prepared in accordance to DIN 50125 Type A 6 mm diameter tensile test piece [36].

The remaining six specimens, three from each group, were subjected to deep rolling. DR was performed on a Spinner CNC lathe using YAMATO SKUV20 roller disk type deep rolling apparatus that was attached to lathe's tool holder. The roller disk has an outer diameter of 85 mm and has a nose radius of 2.5 mm, also the rolling diameter is 15 mm which is equal to the specimen diameter. The DR setup can be seen in Figure 3-1. DR was subjected to specimens with single pass at three different forces given; 1000N, 2000N and 3000N, with a feed rate of 0,1 mm per revolution. The specimens were named after their temper condition and DR force applied to them; specimen naming is given in Table 3-2.

Figure 3-1: Deep Rolling setup.

Table 3-2: Specimen naming.

	DR not applied	1000N	2000N	3000N
T4	T4-AR	T4-1000N	T4-2000N	T4-3000N
T6	T6-AR	T6-1000N	T6-2000N	T6-3000N

Prior to hardness tests, a smooth and polished surface is necessary to observe indentations on the examined surface. DR applied specimens were cut to a specific length with a Metkon MICRACUT 152 precision cutter in order to fit in cold mounting coupon. Then these six specimens were cold casted using epoxy resin and epoxy curing agent. Before surface polishing, all specimens were ground on Metkon FORCIPOL 2V grinder-polisher bench. Grinding was performed using SiC sandpapers with grits P400, P800, P1200 and P2500, respectively. Then, the ground faces of the specimens were polished with monocrystalline diamond suspensions in order of 6 μ and 1 μ. The polished faces of the specimens can be seen in Figure 3-2.

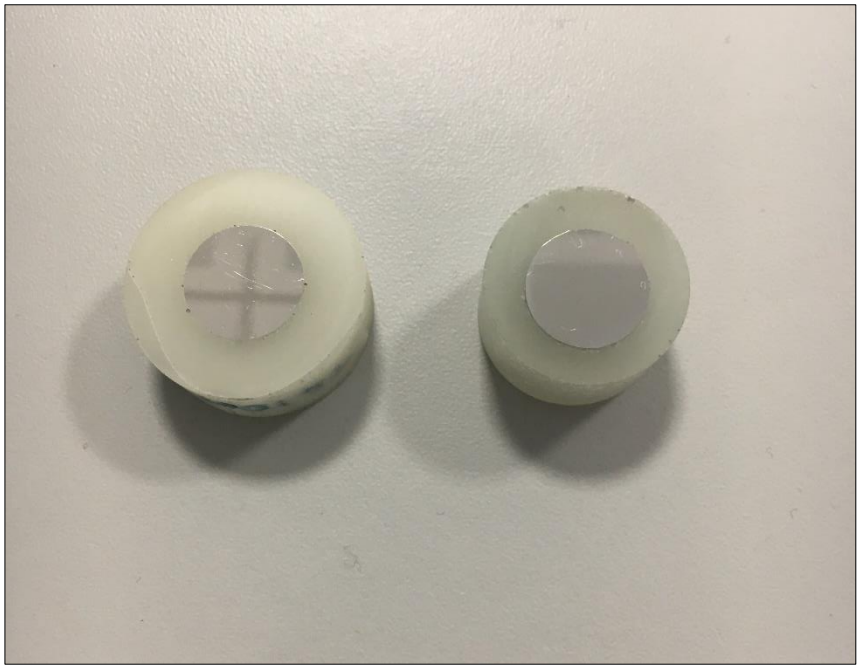

Figure 3-2: Polished faces of the specimens.

Hardness tests were performed to obtain the change in subsurface hardness distribution of the specimens subjected to DR. Since DR does not affect so deep in applied direction, the interested area for hardness tests was narrow and to obtain a distribution, lots of measurements were made. Therefore, Vickers test method for microindentation hardness

evaluation of materials was used for this study and tests were conducted as per ASTM E92-17 and ASTM E384-17 [37, 38].

The hardness measurements were performed on an EMCOTEST DuraScan 20 G5 test bench. Test setup can be seen in Figure 3-3. The indentation force was 10 grams-force (HV0.01) and dwell time was 15 seconds. As specified in standard [38], spacing between adjacent indentations was kept at least 2.5 times the length of the diagonals as shown in Figure 3-4.

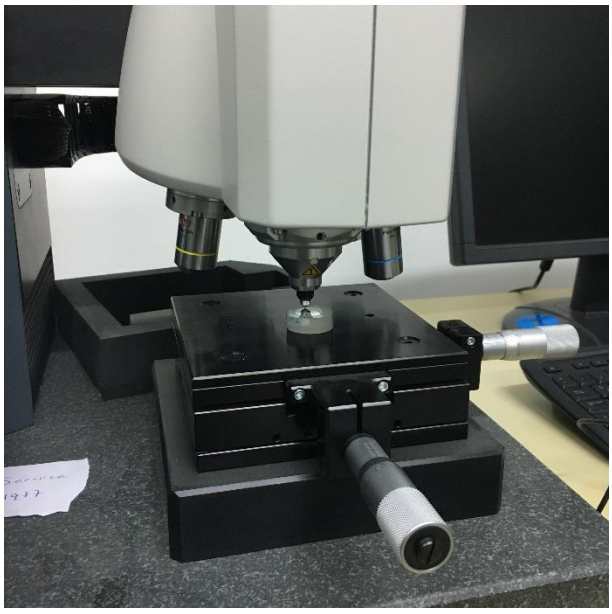

Figure 3-3: Hardness test setup.

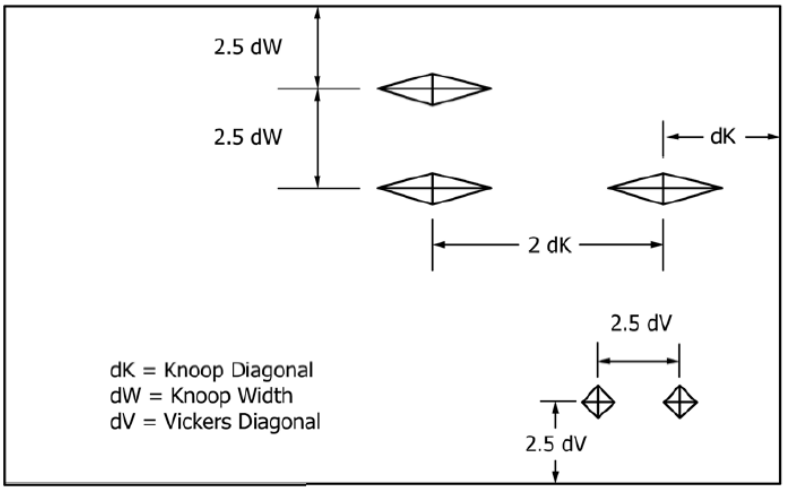

Figure 3-4: Minimum Recommended Spacing for Knoop and Vickers Indentations according to ASTM E384-17 [38].

At first, measurements were taken at specimen cores of the first specimens of each temper group to obtain hardness values of areas that was not exposed to DR. Then, measurements were taken sequentially at specimens' edges in radial direction as shown in Figure 3-6 and recorded. A picture showing measurement of a single indentation is given in Figure 3-7. Measurements were taken up to maximum 3 mm deep in radial direction. The first indentations at edge was taken at 40 μm away from the specimen edge and distance between adjacent indentations was also 40 μm. For each specimen, measurements were repeated at least for once to understand if the hardened layers are uniformly distributed along the circumference and to establish accuracy of measurements.

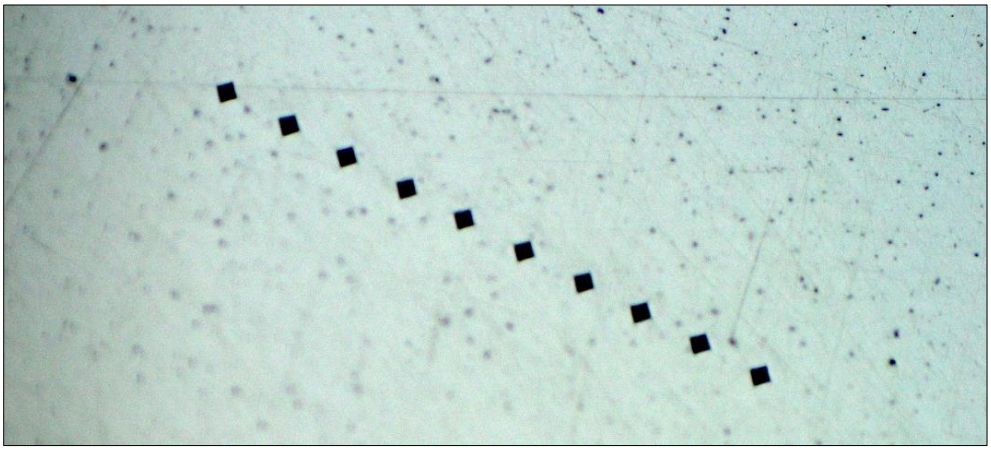

Figure 3-5: Indentations at specimen core.

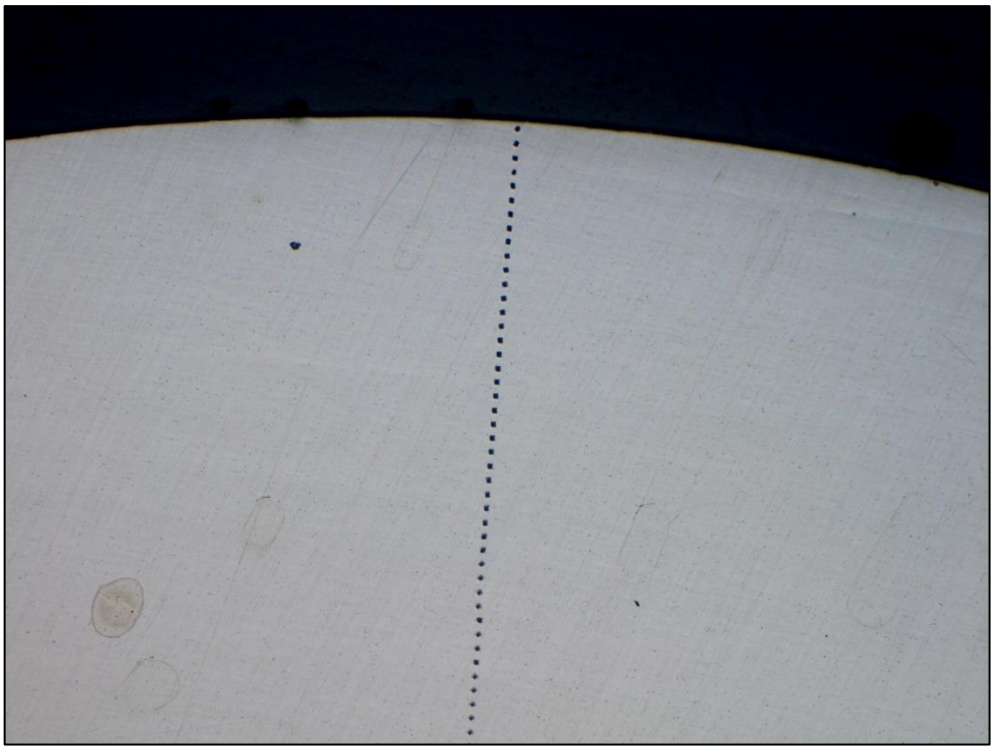

Figure 3-6: Indentations at specimen edge.

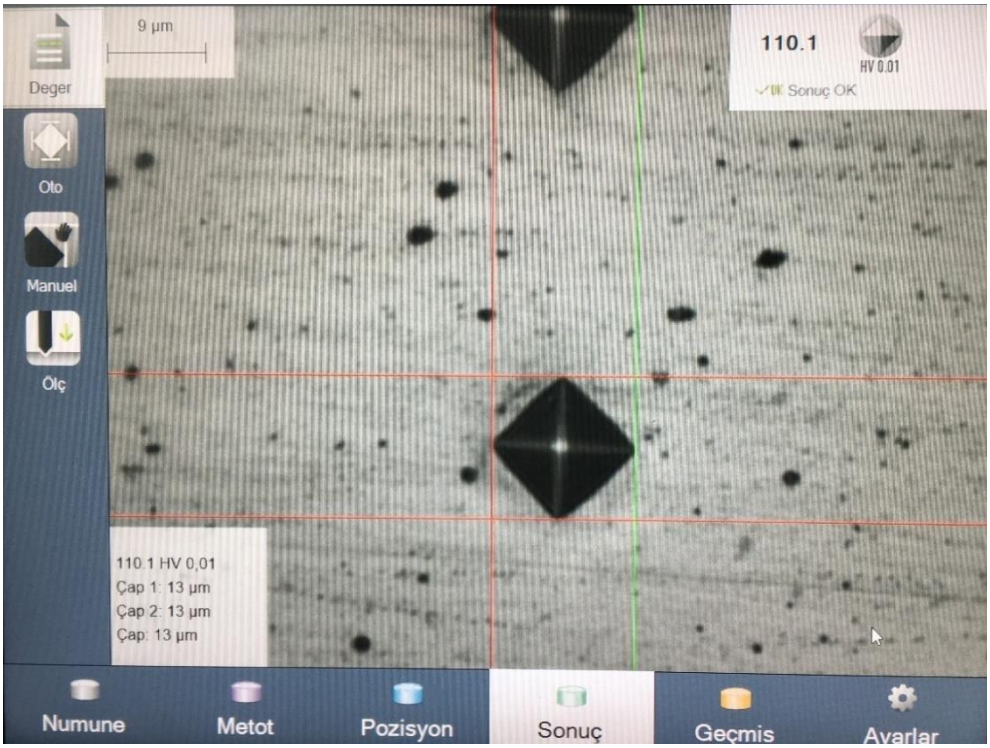

Figure 3-7: Measurement of a single indentation.

In order to understand the effect of DR on surface roughness of the specimens, measurements were performed. The measurements were performed using a Mitutoyo SJ-210 surface roughness tester with a sampling length of 1.25 mm. For each specimen, five

measurements were performed. Measured parameters of surface roughness are as follows [39]. Arithmetical mean height (Ra); which is calculated by taking arithmetical mean of the absolute value of the assessed profile's height. Root mean square deviation (Rq); which is calculated by taking root mean square of heights of the assessed profile. Maximum height of profile (Rz); which is calculated by summing up the largest profile peak's height and the largest profile valley's depth. These parameters were recorded for each specimen and average of five measurements were tabulated. In addition, roughness profiles of these measurements were taken.

In numerical simulations part of the study, several finite element analyses were performed on a work-station computer. The models were prepared using the same material and force variations used in experimental study. The details of analyses models are given in section 5.

The results from experimental studies were evaluated in section 4 and the results from finite element analysis were evaluated in section 5.2. All results were evaluated together in section 6 and briefly discussed.

4. EXPERIMENTAL RESULTS

4.1. Properties of non-DR Specimens

The stress-strain diagrams obtained from tensile tests of specimens that are not deep rolled were given in Figure 4-1. Additionally, yield and tensile strength values for each specimen are given in Table 4-1.

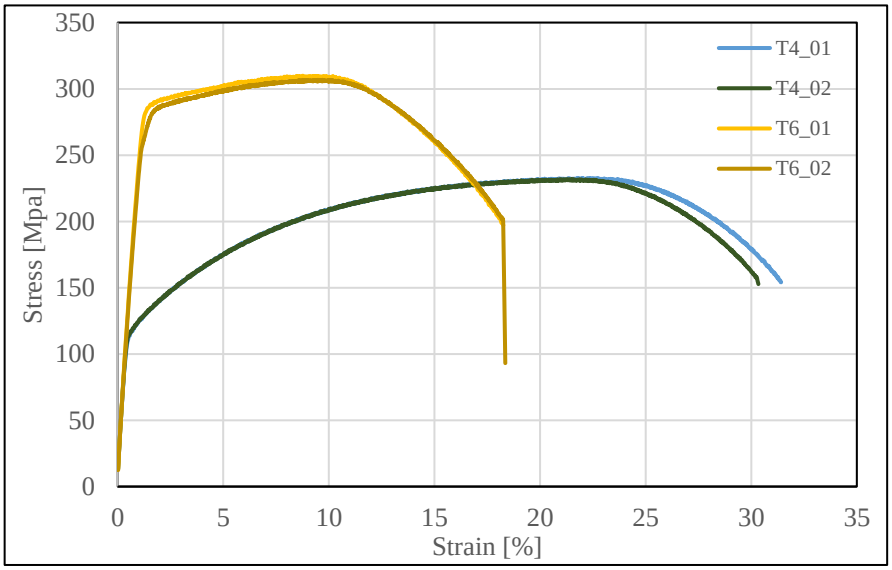

Figure 4-1: Tensile test results of non-DR specimens

Table 4-1: Strength values of tested specimens.

	T4	T6
Yield Strength	117 MPa	282,7 MPa
Tensile Strength	231,8 MPa	308 MPa

As obvious, tensile and yield strength of T6 tempered material is higher than T4 tempered material as expected.

Results of core hardness measurements for each temper condition are given in Table 4-2. These hardness values are used as reference values in evaluation of hardness distributions.

Table 4-2: Average hardness at specimen cores.

Temper group	Hardness, HV 0.01, Average
T4	79,7 ± 5
T6	107,80 ± 5

Again, T6 tempered material shows higher hardness values than T4 tempered material as expected.

4.2. Hardness Distributions

The results of the hardness measurements are given in figures below. Hardness distributions for T4 group are given in figures from Figure 4-2 to Figure 4-5 and hardness distributions for T6 group are given in figures from Figure 4-7 to Figure 4-10. Values given in abscissas shows measurement point's distance from the outer surface of the specimens.

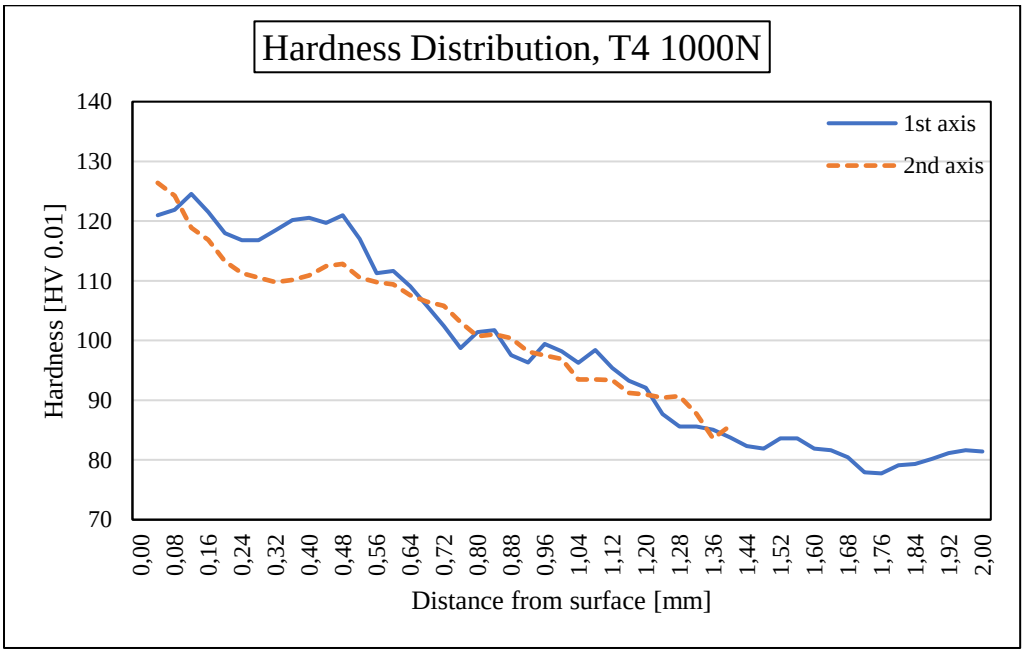

Figure 4-2: Subsurface hardness distribution for specimen T4-1000N.

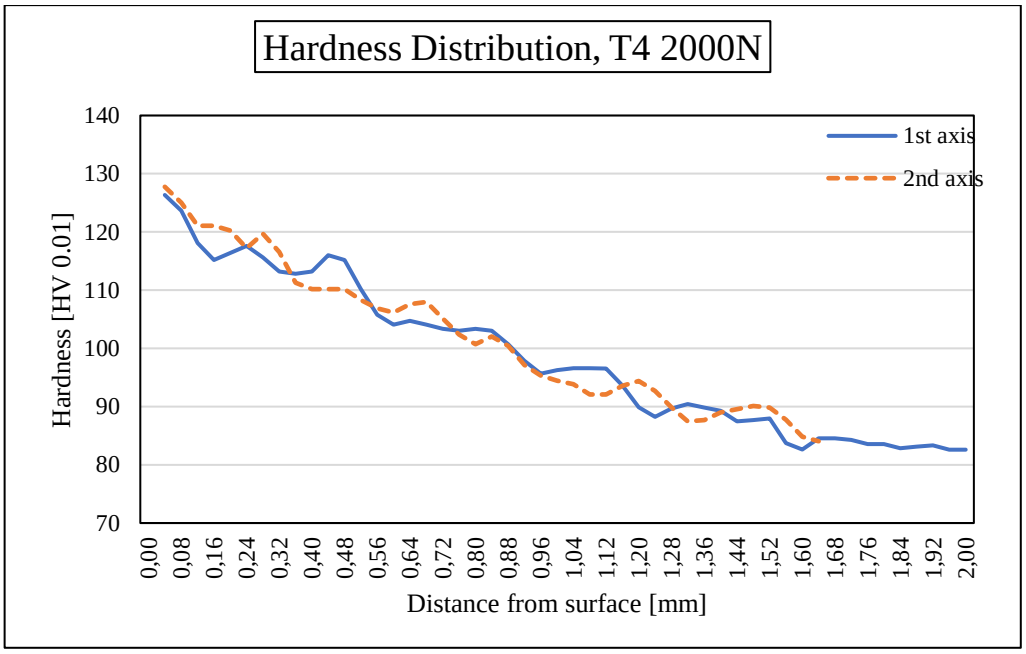

Figure 4-3: Subsurface hardness distribution for specimen T4-2000N.

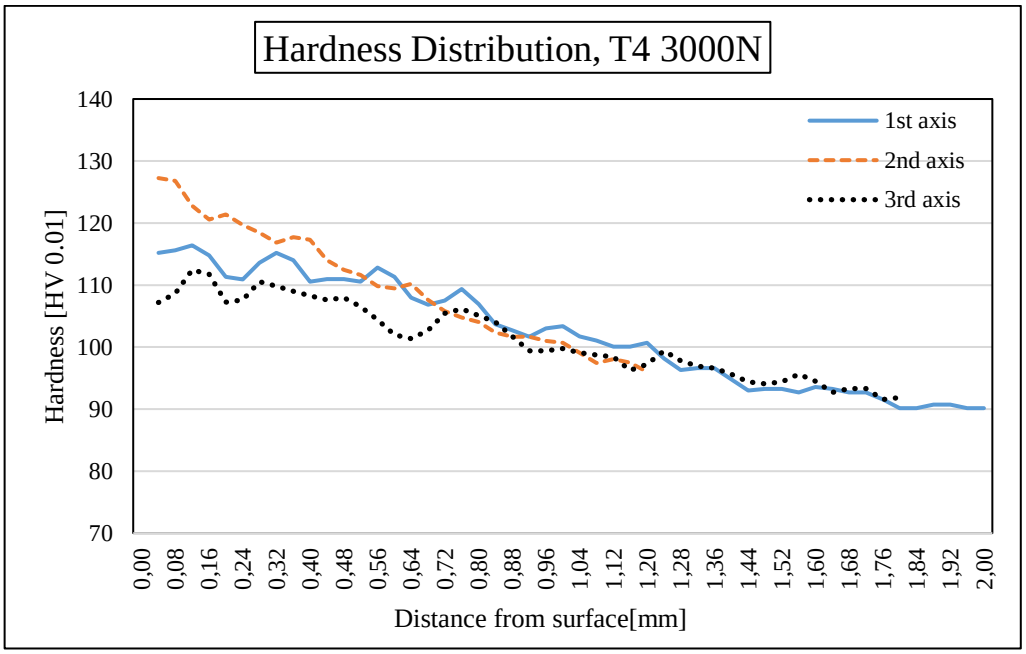

Figure 4-4: Subsurface hardness distribution for specimen T4-3000N.

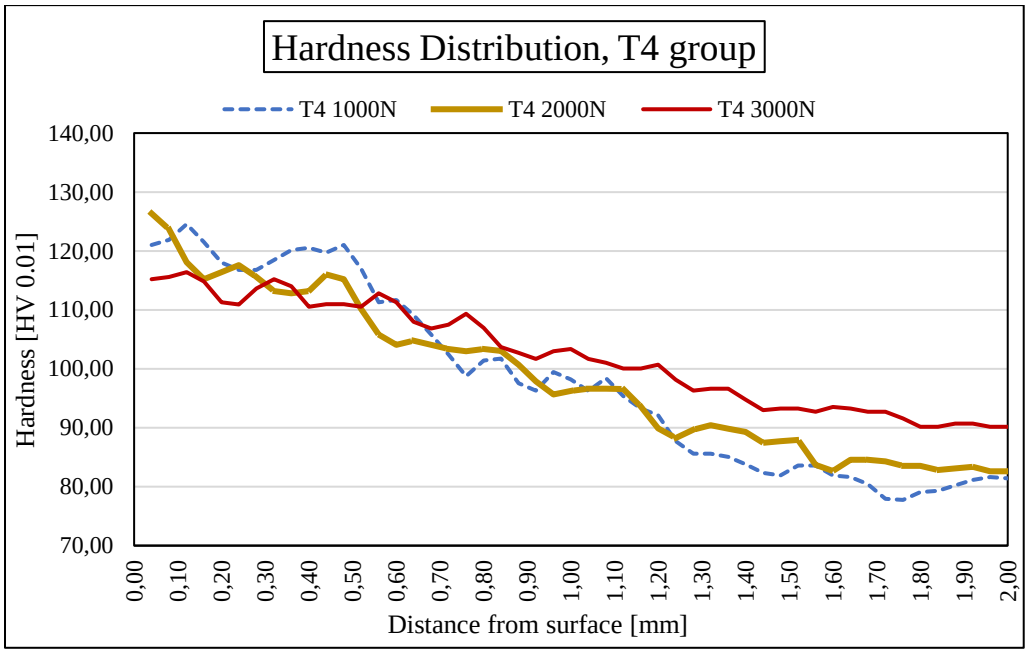

Figure 4-5: Subsurface hardness distribution for T4 group.

As seen in Table 4-2, average hardness value of the area that was not subjected to DR, namely core hardness value, is 79.7 HV 0.01 for T4 group. Examining figures above shows that, for all specimens in T4 group and for all DR forces applied, DR results to an increase in subsurface hardness. Also, the amounts of increase in hardness values for different DR forces applied are close to each other. The peak hardness values obtained are over 120 HV 0.01 except for T4-3000N. For T4-3000N, three measurements were taken to understand the discrepancy between first and second measurements. Clearly, for T4-3000N, hardness values at near surface area are lower than that of T4-1000N and T4-2000N except for the second axis measurement. This situation shows that, for T4-3000N, hardened layers near the surface area may not be uniformly distributed over the circumference. In order to understand why non-uniform distribution happened, microscope images were taken and at near surface are presented in Figure 4-6.

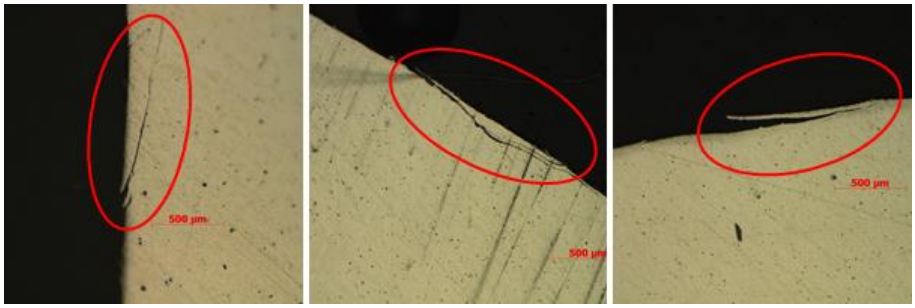

Figure 4-6: Microscope images of near surface cracks for T4-3000N specimen.

In Figure 4-6, surface cracks formed by deep rolling of T4 tempered material at 3000N can be seen clearly. It is obvious, although outmost layers are hardened by deep rolling, these layers were very likely lost at some zones due to cracks formed at surface and near surface area. Therefore, non-uniform distribution of outmost hardened layers showed up most probably due to deterioration of the surface and subsurface area by excessive loading.

On the other hand, hardness values gradually decrease as diverging from outer surface. However, this decrease shows different properties for each force applied. That is, as DR force increases, hardness rise happens in deeper areas and drop to core hardness value can be observed in more distant areas. Drop to core values happened at 1.560 mm for T4-1000N, at 1.920 mm for T4-2000N and at 2.240 mm for T4-3000N, from the outer surface.

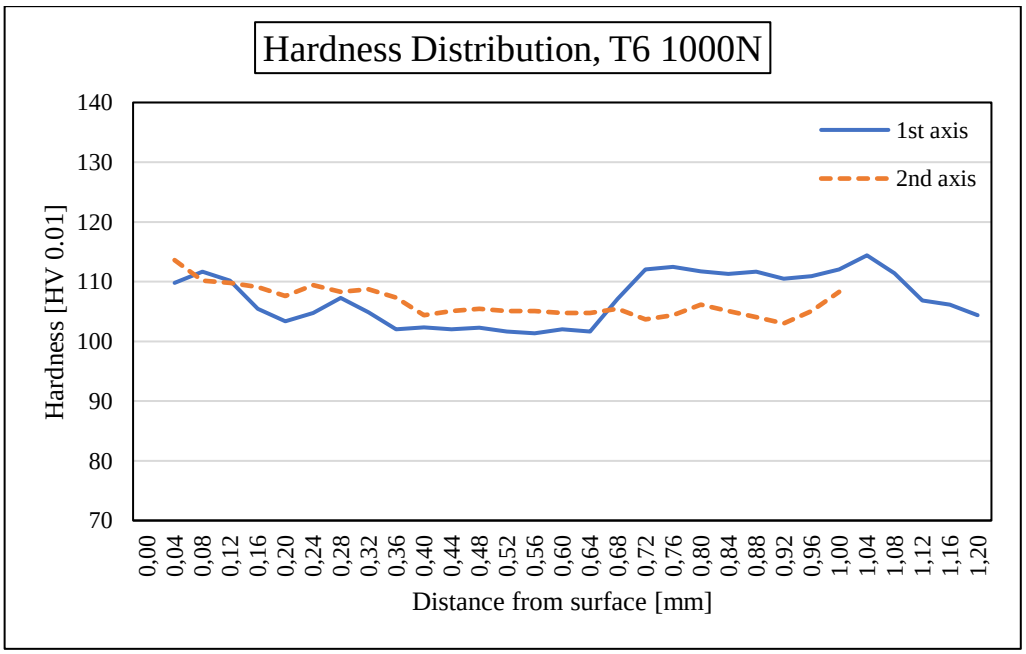

Figure 4-7: Subsurface hardness distribution for specimen T6-1000N.

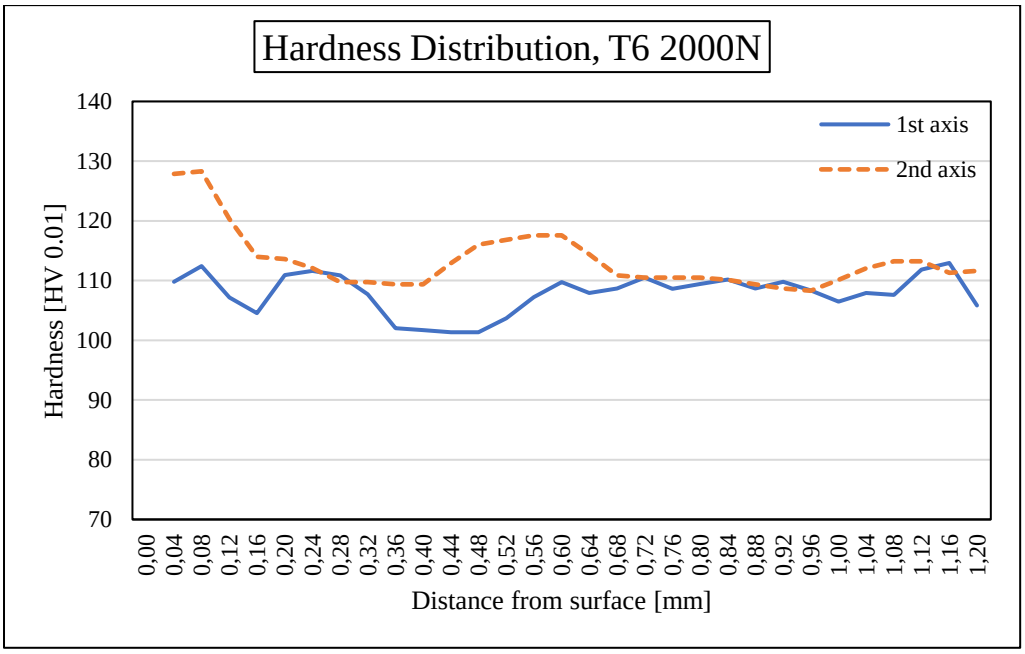

Figure 4-8: Subsurface hardness distribution for specimen T6-2000N.

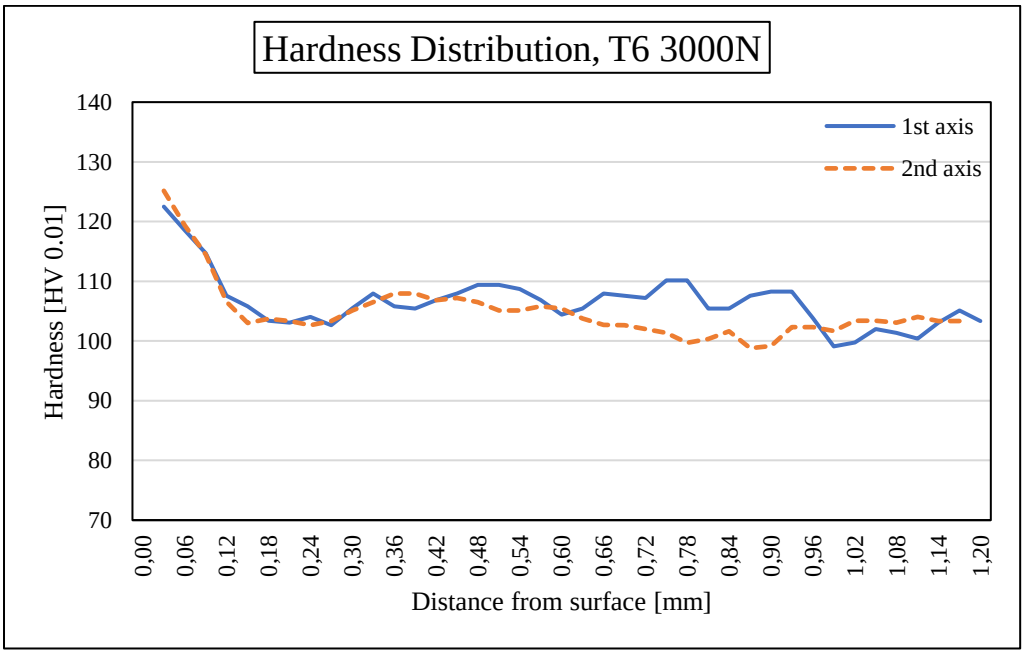

Figure 4-9: Subsurface hardness distribution for specimen T6-3000N.

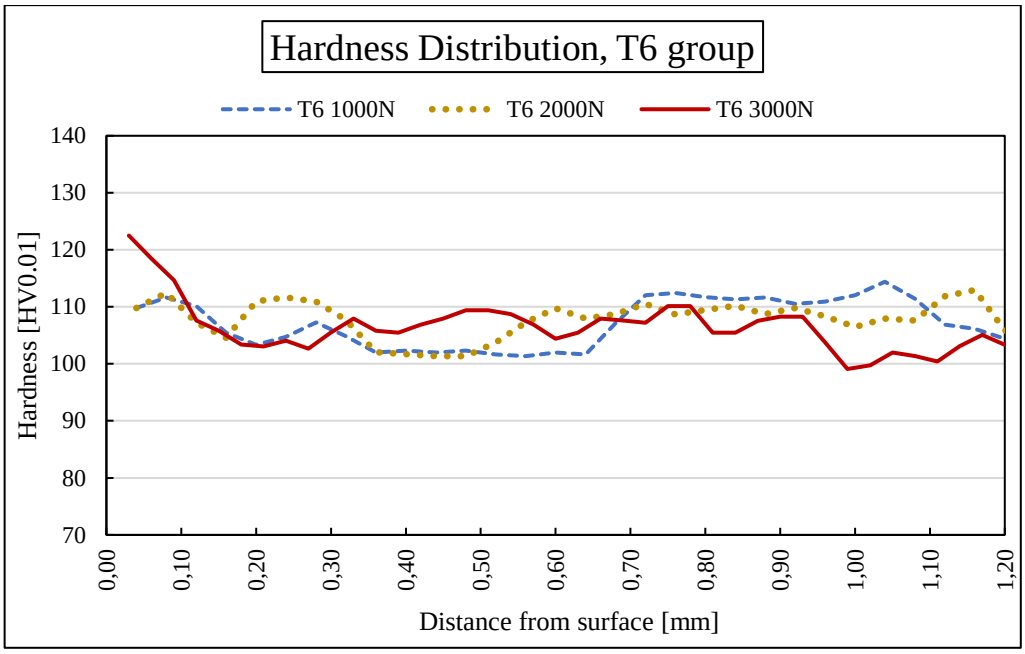

Figure 4-10: Subsurface hardness distribution for T6 group.

From Table 4-2, the core hardness value is 107.80 HV 0.01 for T6 group. It can be seen from figures above, no significant rise in hardness values were obtained for T6-1000 and T6-2000 in a bulk manner. A horizontal behaviour was observed in hardness values for specimens deep rolled at 1000N and 2000N. However, at 3000N DR force, a distinct hardness increase was obtained at near surface area. Yet, a sharp decrease in hardness to core value happens in layers at 0.1 mm depth for T6-3000N. The hardened layer may be thicker than observed in hardness distribution. Because microscope images taken for T6-3000N specimen also showed that cracks exist at near surface area. Again, some hardened layers were probably lost due to cracks formed by excessive loading. These cracks were shown in red circles in Figure 4-11.

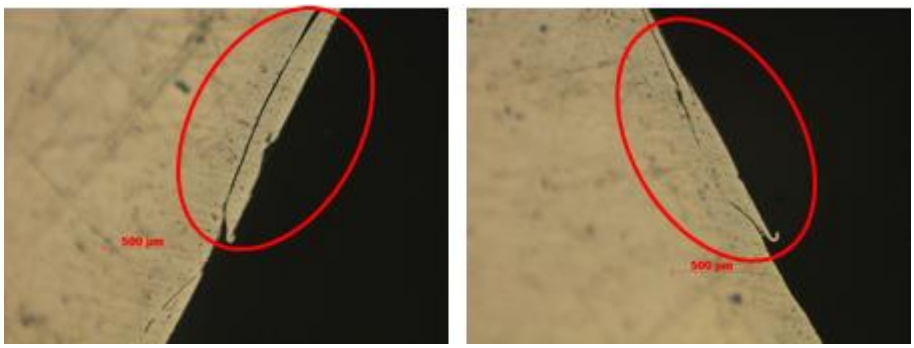

Figure 4-11: Microscope images of near surface cracks for T6-3000N specimen.

On the other hand, there are some narrow regions where slight increases can be seen. For example, as shown in Figure 4-7, a small rise exists between points 0.680 mm and 1.040 mm in first axis measurements. This is most likely caused by coinciding to a precipitate during indentations, because in second axis measurements no such behaviour can be seen in the region mentioned.

4.3. Surface Roughness Results

The measurement results showing Ra, Rq and Rz values are given in Table 4-3. In the first and fifth rows of the Table 4-3, values for T4-AR and T6-AR are given. These values were used as reference values while evaluating the change in surface roughness.

Table 4-3: Ra, Rq and Rz values of all specimens [µm].

	Ra	Rq	Rz
T4-AR	0,449	0,544	2,064
T4-1000N	0,371	0,455	1,737
T4-2000N	0,666	0,850	3,600
T4-3000N	0,684	0,861	3,576
T6-AR	0,881	1,048	3,777
T6-1000N	0,405	0,502	2,008
T6-2000N	0,460	0,577	2,366
T6-3000N	0,492	0,644	2,824

Evaluating the results in Table 4-3 shows that, DR effects are different for each temper group. Considering DR forces, force increase has a negative effect on surface roughness for T4 group. At first, DR applied at 1000N decreases the surface roughness but then with increasing force surface roughness gets higher than T4-AR's surface roughness.

However, for T6 group, surface roughness is lower than T6-AR's surface roughness for all forces applied. Increasing applied force also increases surface roughness for T6 group but, keeps it below T6-AR's surface roughness value.

In addition to surface roughness values, measurement profiles are also given in Figure 4-12 and Figure 4-13.

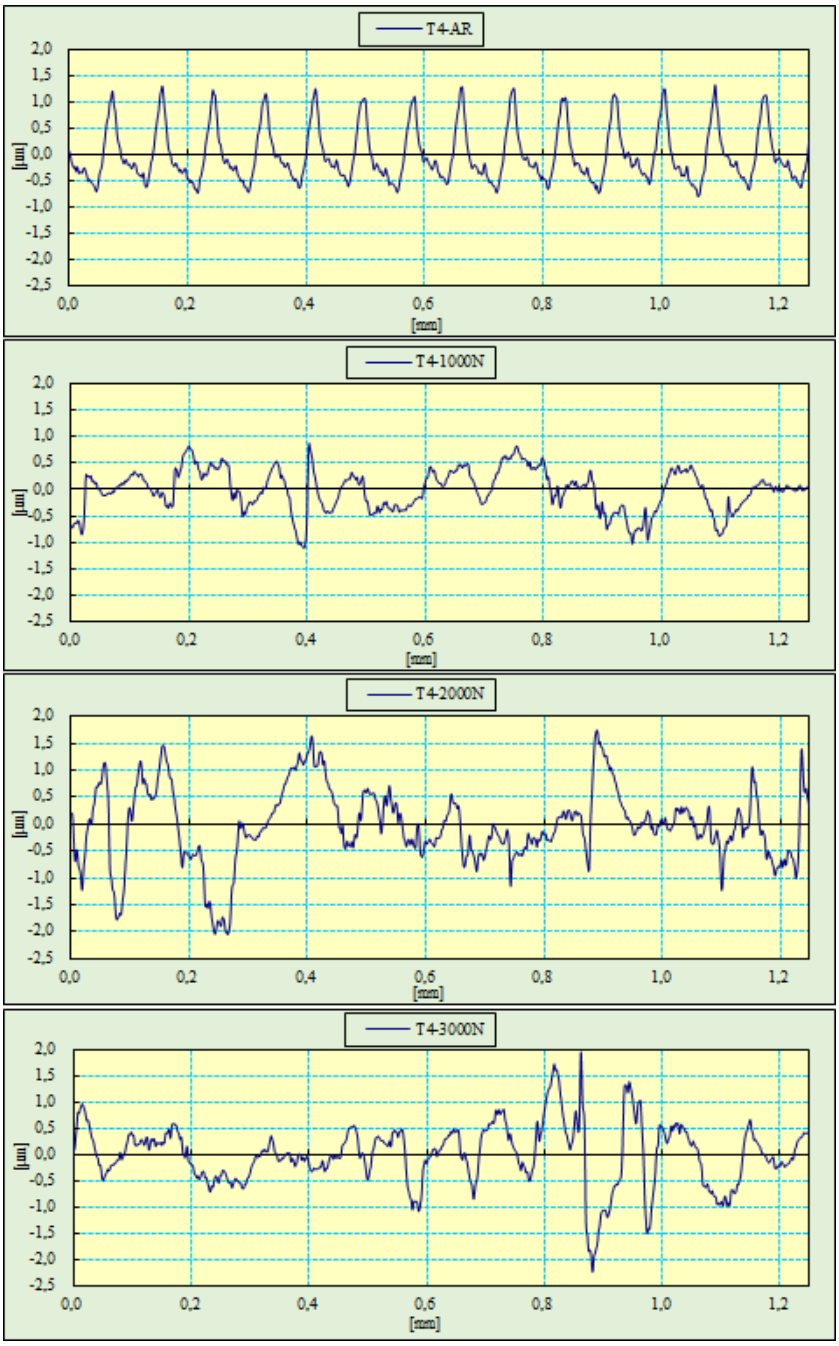

Figure 4-12: Surface roughness profiles for T4 group.

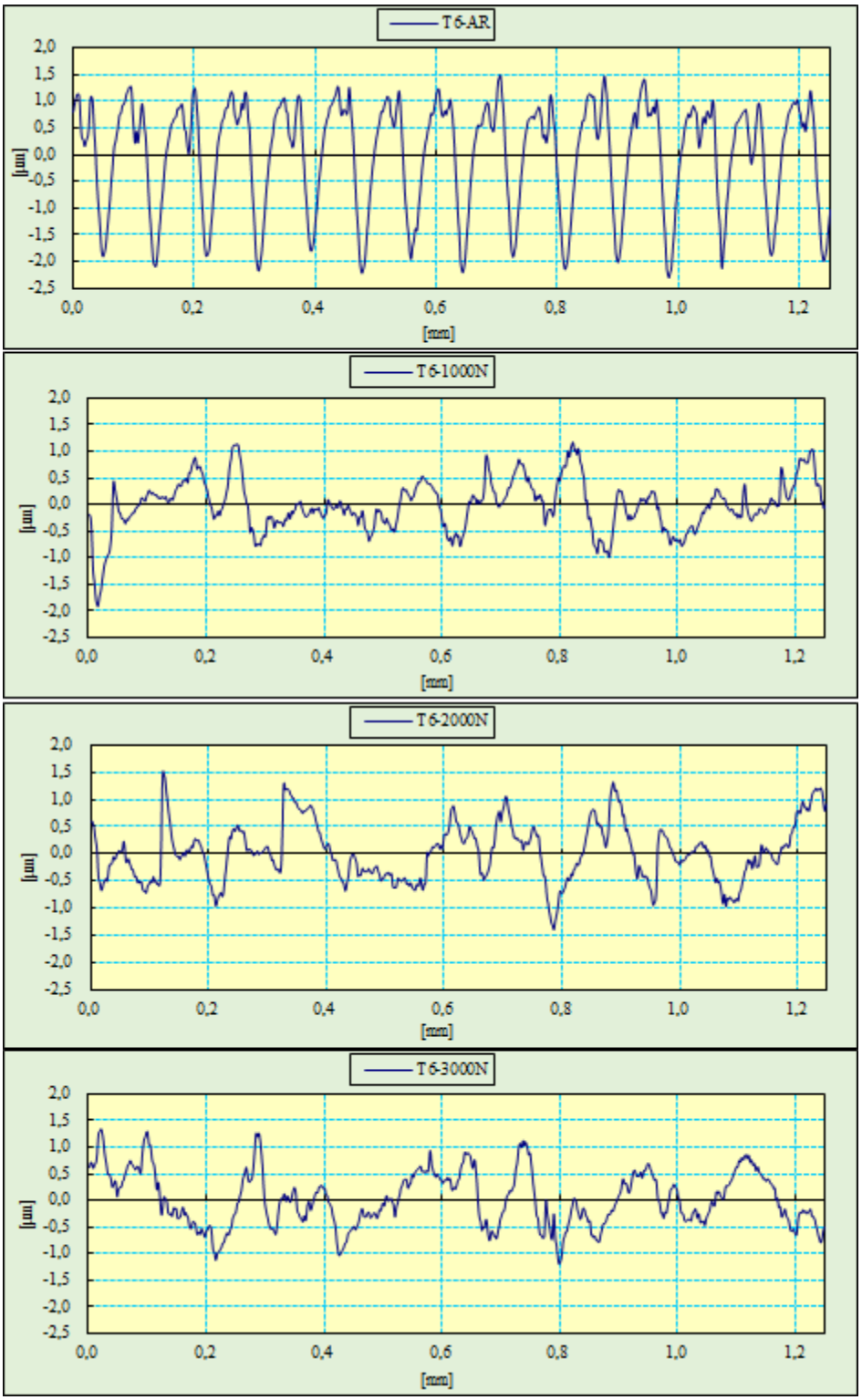

Figure 4-13: Surface roughness profiles for T6 group.

It is clearly seen that, for as-received specimens, namely T4-AR and T6-AR, roughness profiles show a repetitive behaviour. This is most probably caused by machining process done on the lathe, which leaves repetitive marks on subjected material, before subjecting DR to specimens. However, for T4 group valleys are shallow while peaks are high. In

contrary, for T6 group, valleys are deep while peaks are low. Despite the machining were subjected to specimens at same parameters, this difference is most probably caused by different hardness values of T4 and T6 group specimens.

Examining profiles tells that, most of the peaks are lowered for T4 group at 1000N rolling force. However, even the repetitive behaviour was shifted by DR, high peaks and deep valleys were induced at 2000N and 3000N rolling forces. Therefore, increased surface values for T4 group are produced as can be seen in Table 4-3.

Evaluating profiles for T6 group shows that, repetitive behaviour was altered and most of the peaks and valleys were lowered therefore mean values were decreased. Compared to low rolling force, at 2000N and 3000N even new peaks and valleys were induced, the heights and depths are still lower than as-received T6 specimen.

5. FINITE ELEMENT ANALYSIS

5.1. Model Setup

Numerical simulation is a commonly used method to make predictions about and solve engineering problems in many different disciplines. Problems that incorporate nonlinearities are the subject of this method as well as problems which are assumed to be linear. Besides, as mentioned in section 2.3, numerical simulation is a cheaper method compared to real tests and very effective to obtain optimal conditions. So, in this part of the study, numerical simulation was used to examine strain-hardening state and integrity at the surface and subsurface area due to different loading conditions. Apart from all those, while establishing the analysis model used in this study, an analysis model used in a previous study was examined and benefited with the courtesy of its owner [40]. A screenshot showing overall look of the model can be seen in Figure 5-1.

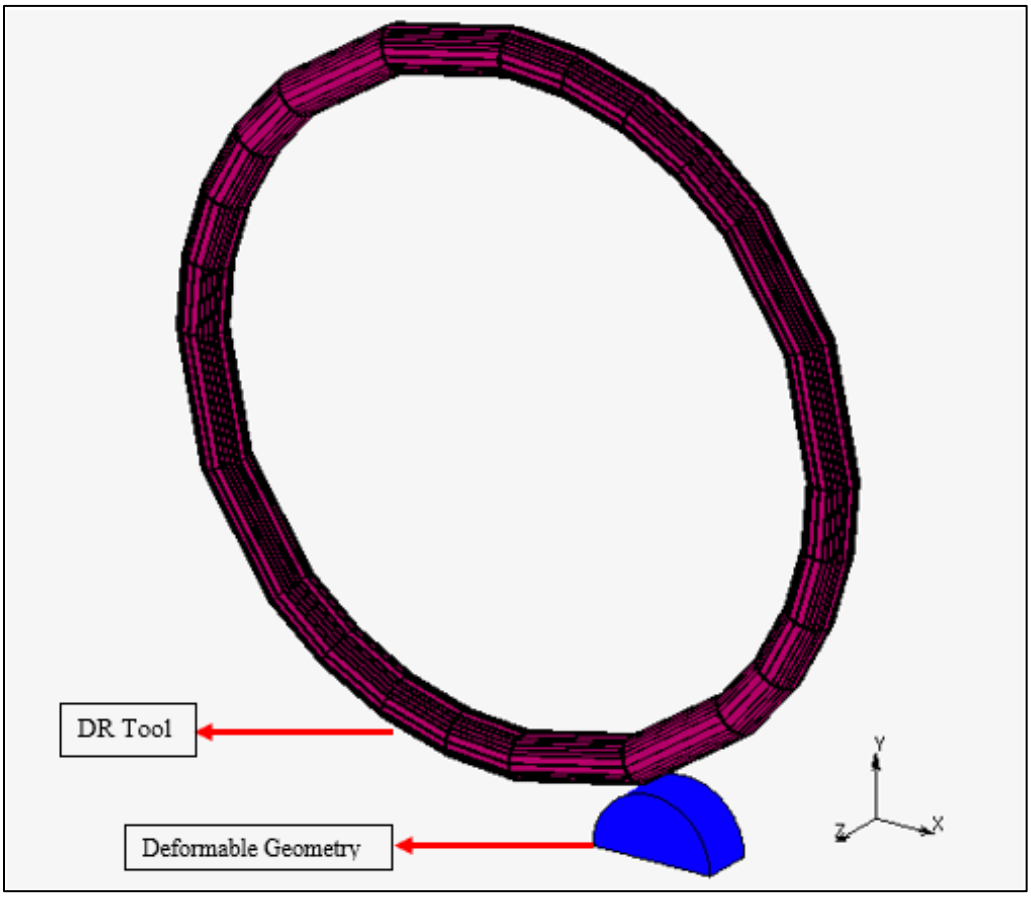

Figure 5-1: Overall look of analysis model.

The component that is subjected to DR was modelled as a deformable geometry and shaped as a semi-cylinder to reduce the element count. The DR tool on the other hand, was modelled as rigid surfaces since it can be assumed as a rigid body compared to DR subjected component. On the other hand, hexahedral elements were used to mesh the deformable geometry. It is a good approach to use fine mesh at areas of special interest, thus element sizes were kept small enough at the deformation zones, as can be seen in Figure 5-2.

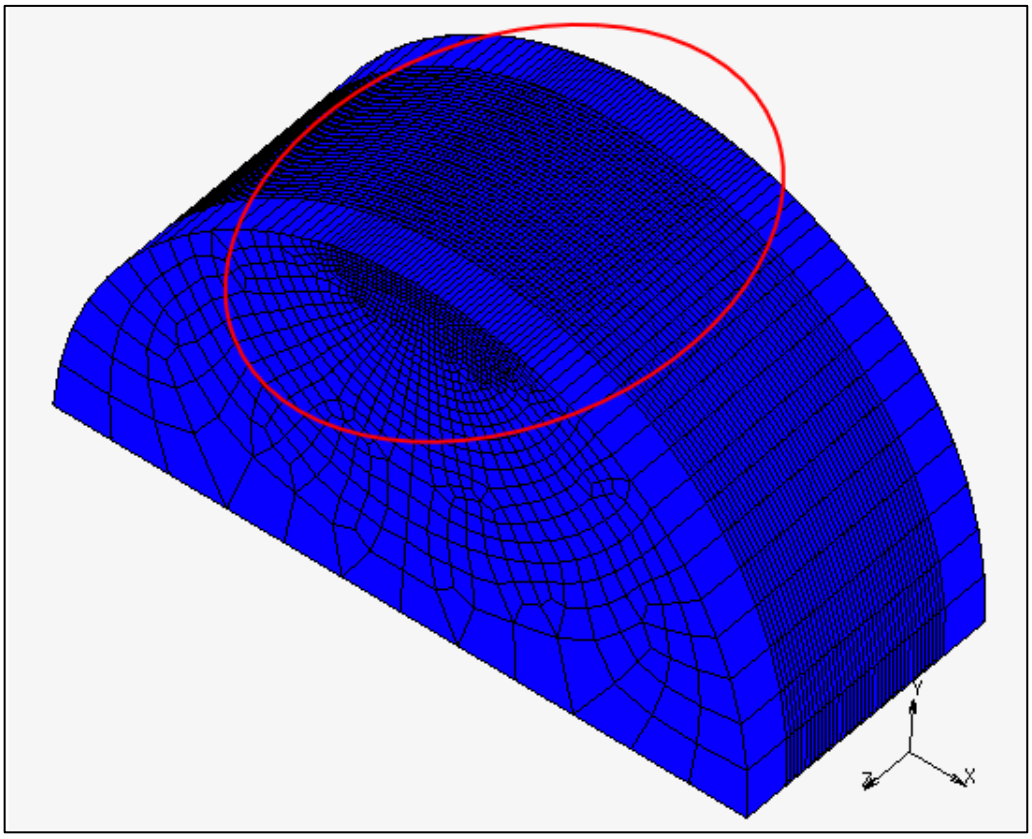

Figure 5-2: Deformable geometry with visible elements.

Analysis time is an important parameter for efficiency concerns and element movement is a time-consuming factor in numerical analysis. Therefore, only tool geometry allowed to move over the deformable geometry while considering relative motion between the tool and the deformable geometry. For this reason, fixed type boundary condition was given to nodes in deformable geometry except its cylindrical surface. Finally, touch type contact was defined between the tool and deformable geometry.

The material for deformable geometry was assigned as elastic-plastic isotropic material and von-Mises yield criterion was used in detection of transition to plastic region.

Besides, isotropic strain hardening law was defined using the actual material's flow curves. In order to obtain material's flow curve, Swift Equation was used. Swift Equation is described as follows [41]:

$$\sigma = K \cdot (\epsilon_0 + \epsilon)^n \qquad (1)$$

Where K, ϵ_0, n represents material constant, initial strain and material hardening exponent, respectively. The material constant K and initial strain ϵ_0, can be calculated as follows.

$$K = \sigma_{UTS} \cdot \left(\frac{e}{n}\right)^n \qquad (2)$$

$$\epsilon_0 = \left(\frac{\sigma_Y}{K}\right)^{\frac{1}{n}} \qquad (3)$$

Where σ_{UTS}, e and σ_Y represents tensile strength, *Euler's number* and yield strength, respectively. In order to obtain above parameters for Swift equation, except material hardening exponent n, tensile test results given in Section 4.1 were used. However, material hardening exponent n is determined using values found in literature and an optimized value for each material was chosen by trial and error until reasonable flow curves were obtained. The flow curves obtained are given Figure 5-3.

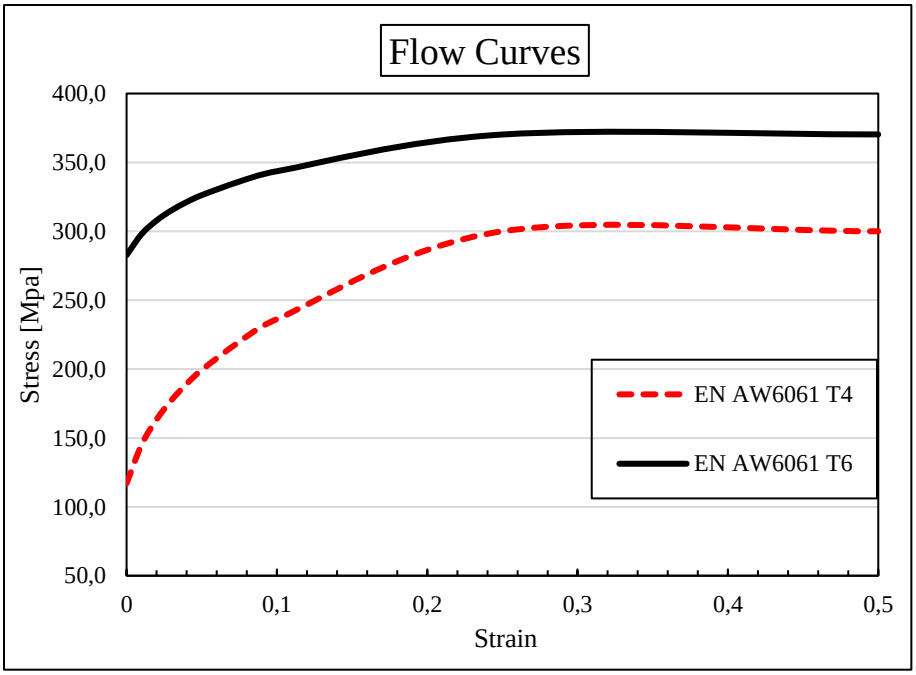

Figure 5-3: Flow curves of the materials.

In addition to plasticity properties, damage property is also defined for the material in order to remark possible damage zones. As damage model, Cockroft-Latham damage indicator, which considers the maximum principal stress, was used. The proposed criterion is given as follows [42]:

$$\int \frac{\sigma_{max}}{\bar{\sigma}} \dot{\bar{\epsilon}} dt \geq C \qquad (4)$$

Where σ_{max}, $\bar{\sigma}$, $\dot{\bar{\epsilon}}$ and C represents maximum principal stress, effective von-Mises stress, effective plastic strain rate and critical material constant, respectively. The critical material constant can vary depending on material, material's strength and plasticity properties. Therefore, in order to obtain the C value, tensile tests or compression tests should be conducted, and results should be compared to numerical simulations. Such tests couldn't be conducted and the C value belonging to materials of interest couldn't be found in literature as well. Yet, it is still possible to evaluate damage results by comparison between cases and reasonable comments can be made with the help of experimental results.

Application of load cases is also an important factor to obtain accurate results from analysis. The load is applied from tool centre towards the component's centre and the load vector was re-oriented as tool rolls over the component as shown in Figure 5-4. The tool's centre follows the path shown by the dashed line. It also rotates about its own centre axis in the direction shown in figure. The total application of load is divided into five load cases such that at each load case a certain section was covered. Then the tool was shifted 0,1 mm in +Z direction as shown in Figure 5-5 and the same procedure was repeated until five load cases were applied.

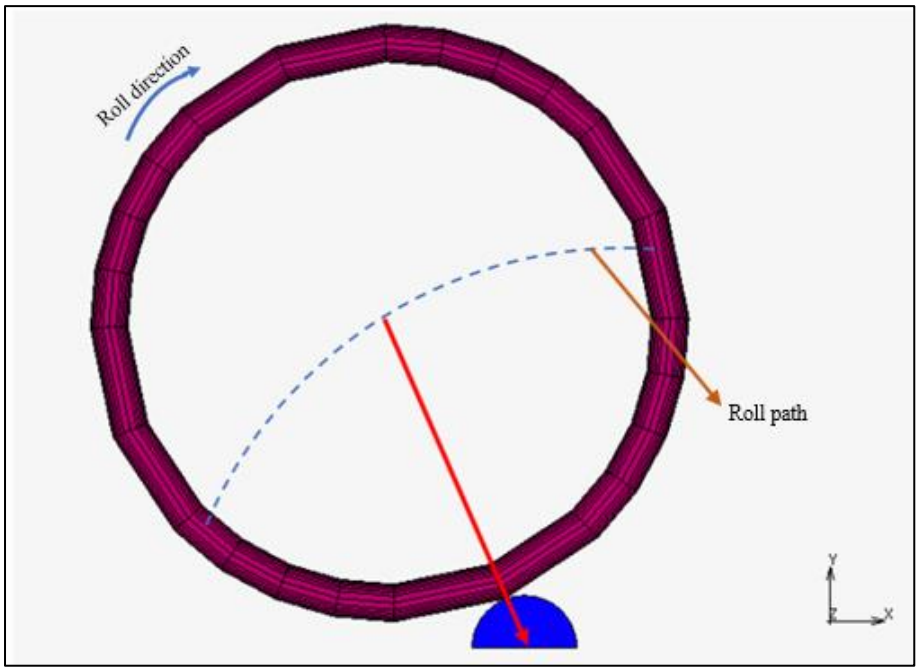

Figure 5-4: An illustration showing load application direction.

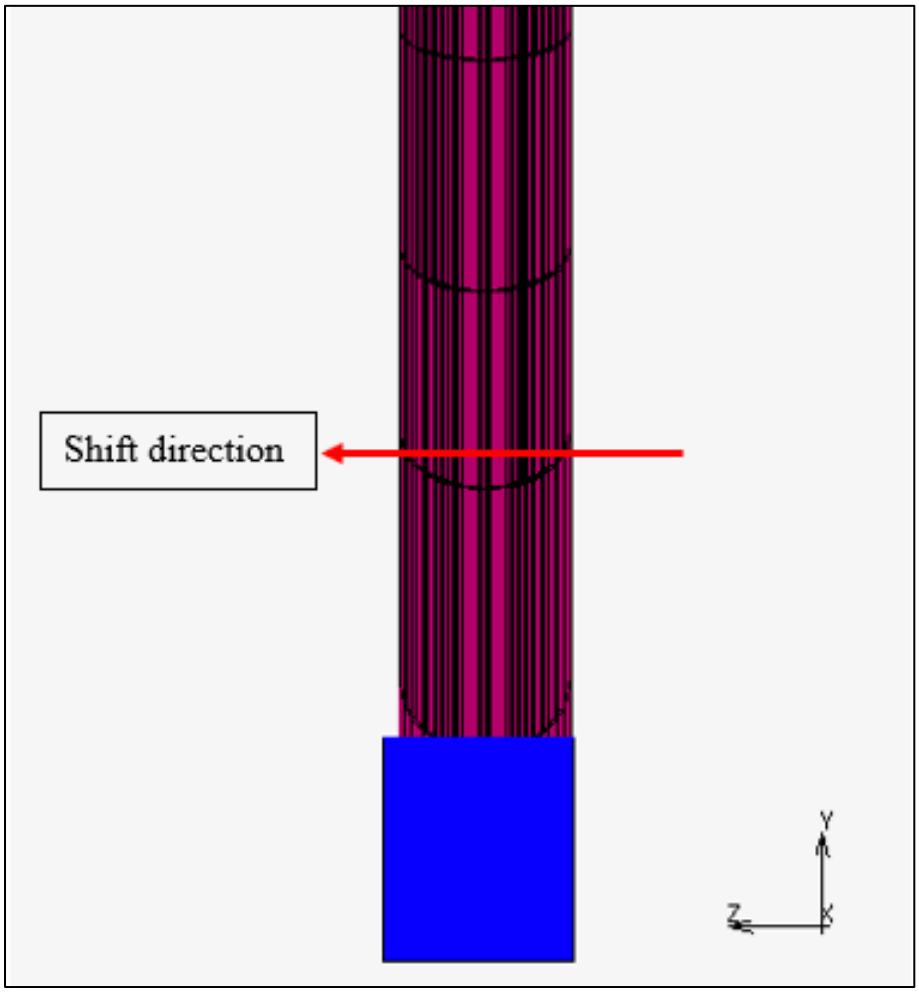

Figure 5-5: An illustration showing tool shift direction.

Finally, in order to evaluate component's behaviour after DR, total equivalent plastic strain (TEPS) and damage results were requested from the analysis. The same combination of DR force and material in section 4 were applied in numerical simulation part of the study. So, six analysis models were prepared and run in total.

5.2. Simulation Results

In order to evaluate simulations, results were extracted using software's result plotting interfaces. A sample graphic showing contours of TEPS is given in Figure 5-6.

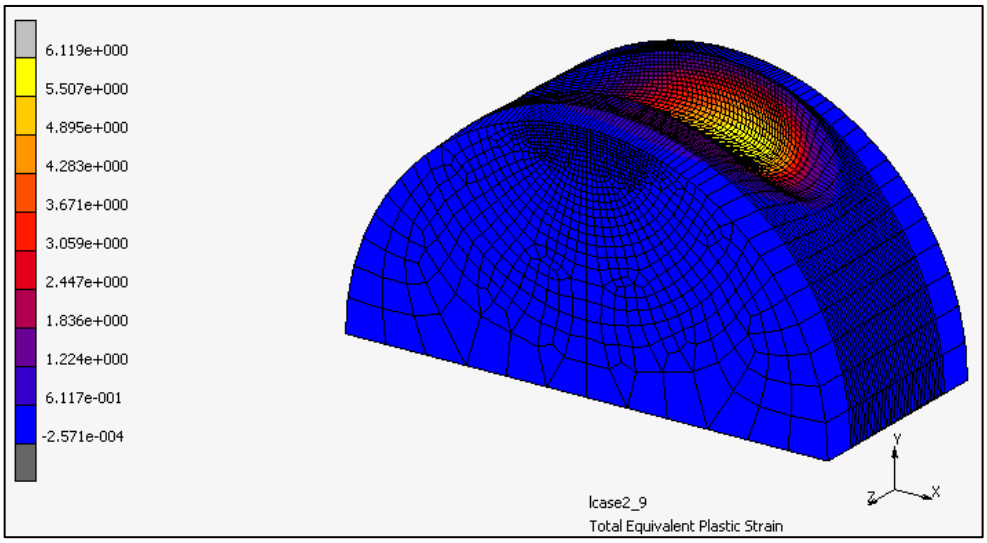

Figure 5-6: Sample result plot showing TEPS contours.

There are two main scalars extracted from the analysis carried out; TEPS and damage. In order to take results, the deformable geometry was cut in half and values at the nodes were printed to a table starting from the node that has the highest value. This procedure is illustrated in Figure 5-7 and Figure 5-8.

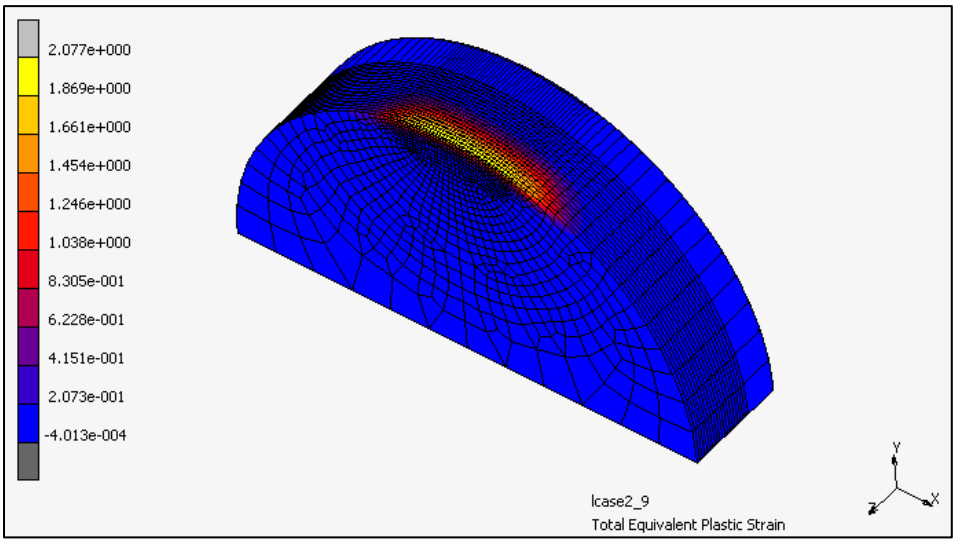

Figure 5-7: Clipped view of deformable geometry.

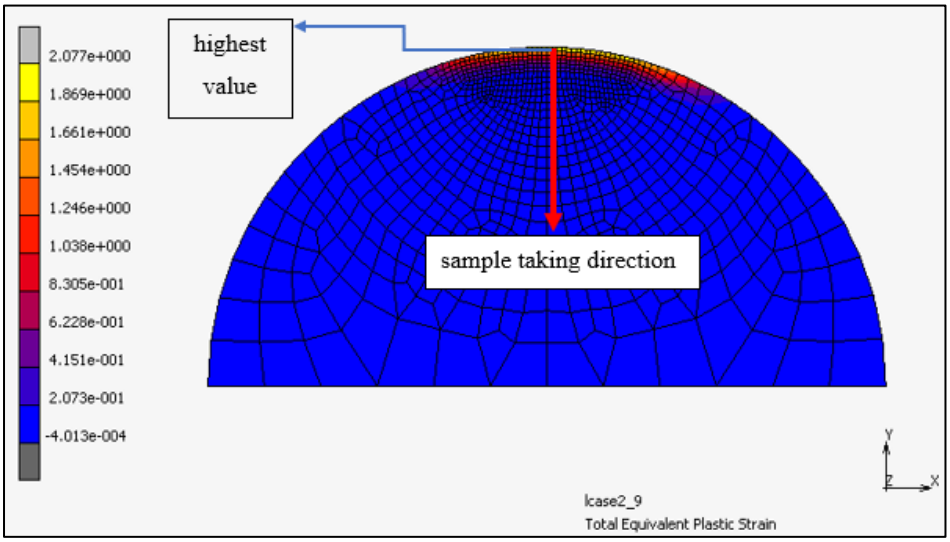

Figure 5-8: An illustration that shows how values were taken.

Later, results were gathered, and alterations are presented as graphs for both material groups. Firstly, TEPS graphs for both material groups are given in Figure 5-9.

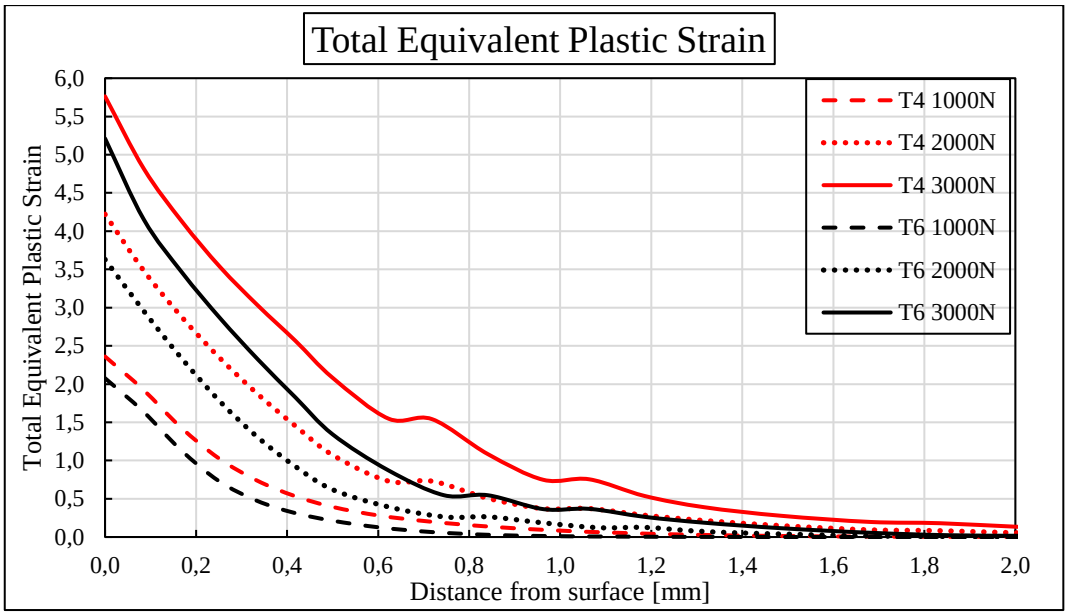

Figure 5-9: Total equivalent plastic strain results for all cases.

As can be seen in Figure 5-9, T4-3000N has the highest TEPS value while T6-1000N has the lowest TEPS value. Also, TEPS value increases for each material group with increased DR force, as expected. Again, within the same material group, plastic strain occurred in deeper areas with increased DR force. In addition, for each force level, plastic strain occurred in deeper areas for T4 group also, T4 group shows higher TEPS values compared to T6 group.

Secondly, damage graphs for both material groups are given in Figure 5-10.

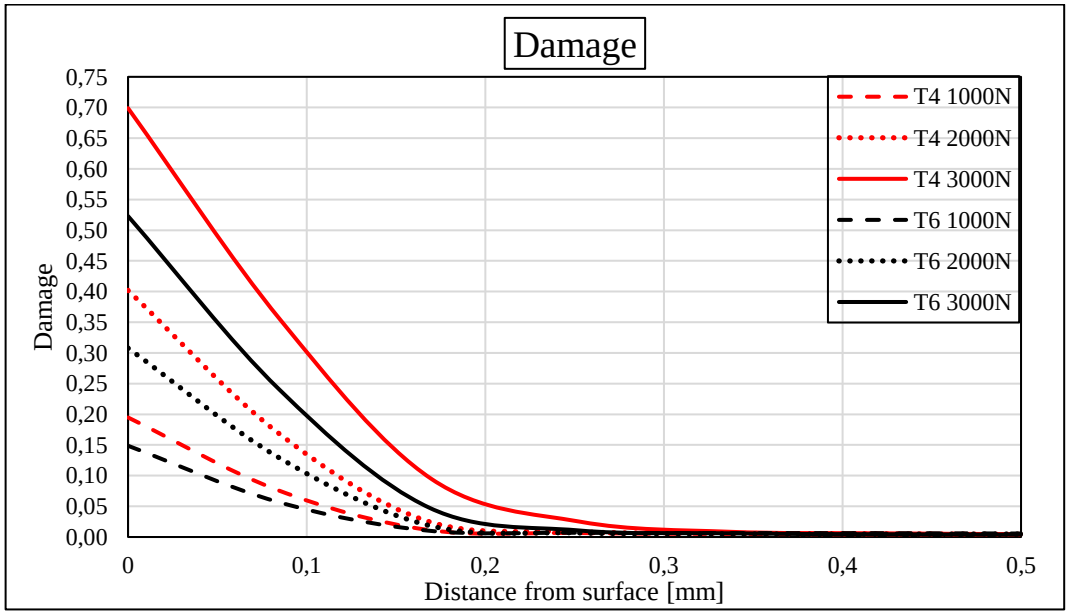

Figure 5-10: Damage results for all cases.

Damage results can be evaluated by looking only to maximum values. Within the same material group, highest damage values were seen at 3000N rolling force, but the highest damage value belongs to T4-3000N case. Besides, for both materials, increased rolling force causes increase in damage values. However, within same force level, damage values of T4 group are always higher than T6 group.

6. DISCUSSION

In experimental part of the study, DR was applied at three different forces to materials in two different temper conditions and six specimens were produced in total. Surface and subsurface hardness measurements and surface roughness measurements were conducted for these six specimens. Finite element analyses were performed using the same material and force variations and TEPS and damage results were obtained for six different cases. Results of experimental work and finite element analyses were evaluated individually. Overall conclusions about these results were discussed as follows.

According to the numerical simulations, TEPS is increased with increasing DR force for T4 group. Also, TEPS rise is nearly proportional to increase in DR force. However, considering hardness distributions for this group, force increase didn't cause a proportional increase in hardness values. Contrarily, level of rise was close to each other for all force values. Basically, it can be said that no further strain-hardening could be accomplished at forces above 1000N. Yet, higher forces provide hardness increase at deeper areas which can be predicted from TEPS results. Apart from these, damage results show that T4-3000N has the highest damage value. This situation was showed itself first by lower hardness values than T4-1000N and T4-2000N at near surface area. After taking microscope images, it was observed that cracks were formed at surface and near surface area. Due to these cracks, hardened layers were very likely lost as flakes at some zones and led to lower hardness values seen in near surface area. This tells us that material's formability limit was exceeded, and surface integrity was not conserved for T4-3000N.

Surface roughness results for T4 tempered material support above considerations as well. Roughness values were dramatically increased at higher forces. The cracks formed by excessive loading can cause spalling at surface hence can leave cavities at the surface. In addition, it is very likely that the flakes formed due to spalling can adhere to surface hence can leave ridges at the surface. Therefore, these cavities and ridges can easily ruin the surface and lead the roughness profile to highly deviate from mean profile line thereby can cause increase in measured parameters of the roughness profile. So, the cracks and flakes formed by excessive loading can be addressed as common cause for decreased

hardness values at near surface and increased surface roughness values and irregular roughness profile for specimen rolled at highest force.

TEPS results for T6 group shows a similar behaviour to T4 group results. However, hardness measurements show that an overall hardness rise for T6 group couldn't be obtained. There exists a small exception that is, for T6-3000N, hardness rise was obtained at a narrow area near the surface of the specimen. Yet, by looking near surface microscope images, it can be said that there could be a thicker area of hardened material. But probably this area was also lost due to cracks formed by excessive loading. These results reveal that to obtain a bulk hardness rise for T6 tempered material, higher plastic strains were needed. On the other hand, highest damage value observed for T6 group is nearly 1.4 times lower than highest damage value observed for T4 group. Yet damage value predicted for T6-3000N is in the second rank. With above considerations about hardness values and microscope images, one can say that material's formability limit was exceeded in near surface area at highest rolling force. Surface roughness profile at highest force also shows an irregular behaviour. Besides, values of the roughness parameters were also increased compared to lower forces. The cracks formed by excessive loading can also cause to form cavities and ridges at the surface. Thus, can be cause of the irregular roughness profile, increased surface roughness for specimen rolled at highest force.

By evaluating the results of this very study, one can say that increasing DR force provides deeper strain-hardened layers, but further hardening can't be accomplished by higher forces. In fact, excessive force may cause deterioration of the surface and may lead to even lower hardness values than those obtained with lower forces, as in agreement with the literature. Additionally, it is apparent that high hardness prior to DR caused DR to be ineffective on hardness increase, which is also in agreement with the literature. Apart from these, surface roughness of the softer material is very sensitive to force rise however, harder material shows better surface roughness at increased forces.

Within this study, a few surface and subsurface characteristics of two differently tempered materials were examined after DR at different forces. Examination of microstructure at surface and subsurface area is needed to fully explain changes in hardness distributions caused by process parameters. Because as well as grain size, density and distribution of dislocations are also main factors which influences a material's

strength. Further studies may include simultaneous investigation of strength and conductivity characteristics of deep rolled parts and evaluation of their microstructural alterations. Besides, these studies can be diversified with varying process parameters and conductor materials.

7. REFERENCES

1. Kiessling, F., *Overhead power lines : planning, design, construction*. Power systems. 2003, Berlin ; New York: Springer. xxviii, 759 p.
2. Sabirov, I., M.Y. Murashkin, and R.Z. Valiev, *Nanostructured aluminium alloys produced by severe plastic deformation: New horizons in development.* Materials Science and Engineering: A, 2013. **560**: p. 1-24.
3. Altenberger, I. *Deep rolling–the past, the present and the future*. in *Conf Proc: ICSP*. 2005.
4. Delgado, P., et al., *State of the art of Deep Rolling.* Precision Engineering-Journal of the International Societies for Precision Engineering and Nanotechnology, 2016. **46**: p. 1-10.
5. Callister, W.D. and D.G. Rethwisch, *Materials science and engineering : an introduction*. 8th ed. 2010, Hoboken, NJ: John Wiley & Sons. xxiii, 885, 82 p.
6. Aluminum Association., *Aluminum electrical conductor handbook*. 3rd ed. 1989, Washington, D.C.: Aluminum Association.
7. British Standards Institution., *BS EN 50183:2000 Conductors for overhead lines. Aluminium-magnesium-silicon alloy wires*. 2000, British Standards Institution.
8. Murashkin, M.Y., et al., *Enhanced mechanical properties and electrical conductivity in ultrafine-grained Al alloy processed via ECAP-PC.* Journal of Materials Science, 2013. **48**(13): p. 4501-4509.
9. Liu, C.H., et al., *Enhancing electrical conductivity and strength in Al alloys by modification of conventional thermo-mechanical process.* Materials & Design, 2015. **87**: p. 1-5.
10. Sauvage, X., et al., *Optimization of electrical conductivity and strength combination by structure design at the nanoscale in Al-Mg-Si alloys.* Acta Materialia, 2015. **98**: p. 355-366.
11. Lipinska, M., P. Bazarnik, and M. Lewandowska, *The influence of severe plastic deformation processes on electrical conductivity of commercially pure aluminium and 5483 aluminium alloy.* Archives of Civil and Mechanical Engineering, 2016. **16**(4): p. 717-723.
12. Aluminum Association., *Aluminum Standards and Data*. 2013, Arlington, VA: Aluminum Association.
13. Valiev, R.Z., M.Y. Murashkin, and I. Sabirov, *A nanostructural design to produce high-strength Al alloys with enhanced electrical conductivity.* Scripta Materialia, 2014. **76**: p. 13-16.
14. Salazar-Guapuriche, M.A., et al. *Correlation of strength with hardness and electrical conductivity for aluminium alloy 7010*. in *Materials science forum*. 2006. Trans Tech Publ.
15. Bobruk, E., et al., *Aging behavior and properties of ultrafine-grained aluminum alloys of Al-Mg-Si system.* Rev. Adv. Mater. Sci, 2012. **31**: p. 109-115.
16. Valiev, R.Z., et al., *Bulk Nanostructured Metals for Innovative Applications.* JOM, 2012. **64**(10): p. 1134-1142.
17. Roven, H.J., et al., *Mechanical properties of aluminium alloys processed by SPD: Comparison of different alloy systems and possible product areas.* Materials Science and Engineering: A, 2005. **410-411**: p. 426-429.

18. Sauvage, X., M. Murashkin, and R. Valiev, *Atomic scale investigation of dynamic precipitation and grain boundary segregation in a 6061 aluminium alloy nanostructured by ECAP*. Kovove Mater, 2011. **49**(1): p. 11.
19. Valiev, R., et al., *On the origin of the extremely high strength of ultrafine-grained Al alloys produced by severe plastic deformation.* Scripta Materialia, 2010. **63**(9): p. 949-952.
20. Cheng, S., et al., *Optimizing the strength and ductility of fine structured 2024 Al alloy by nano-precipitation.* Acta Materialia, 2007. **55**(17): p. 5822-5832.
21. Zhao, Y.-H., et al., *Simultaneously increasing the ductility and strength of nanostructured alloys.* Advanced Materials, 2006. **18**(17): p. 2280-2283.
22. Abrão, A., et al., *The influence of heat treatment and deep rolling on the mechanical properties and integrity of AISI 1060 steel.* Journal of Materials Processing Technology, 2014. **214**(12): p. 3020-3030.
23. Wagner, L., *Mechanical surface treatments on titanium, aluminum and magnesium alloys.* Materials Science and Engineering: A, 1999. **263**(2): p. 210-216.
24. Juijerm, P. and I. Altenberger, *Fatigue behavior of deep rolled Al–Mg–Si–Cu alloy at elevated temperature.* Scripta Materialia, 2006. **55**(10): p. 943-946.
25. Nikitin, I., et al., *High temperature fatigue behavior and residual stress stability of laser-shock peened and deep rolled austenitic steel AISI 304.* Scripta Materialia, 2004. **50**(10): p. 1345-1350.
26. Juijerm, P. and I. Altenberger, *Effective boundary of deep-rolling treatment and its correlation with residual stress stability of Al–Mg–Mn and Al–Mg–Si–Cu alloys.* Scripta Materialia, 2007. **56**(9): p. 745-748.
27. Juijerm, P., I. Altenberger, and B. Scholtes, *Fatigue and residual stress relaxation of deep rolled differently aged aluminium alloy AA6110.* Materials Science and Engineering: A, 2006. **426**(1): p. 4-10.
28. Juijerm, P., I. Altenberger, and B. Scholtes, *Influence of ageing on cyclic deformation behavior and residual stress relaxation of deep rolled as-quenched aluminium alloy AA6110.* International Journal of Fatigue, 2007. **29**(7): p. 1374-1382.
29. Majzoobi, G.H., K. Azadikhah, and J. Nemati, *The effects of deep rolling and shot peening on fretting fatigue resistance of Aluminum-7075-T6.* Materials Science and Engineering a-Structural Materials Properties Microstructure and Processing, 2009. **516**(1-2): p. 235-247.
30. Scheil, J., et al. *Influence of process parameters on surface hardening in hammer peening and deep rolling*. in *Key Engineering Materials*. 2013. Trans Tech Publ.
31. Abrão, A., et al., *The influence of deep rolling on the surface integrity of AISI 1060 high carbon steel.* Procedia CIRP 13 (2014), 2014. **13**: p. 31-36.
32. Nalla, R., et al., *On the influence of mechanical surface treatments—deep rolling and laser shock peening—on the fatigue behavior of Ti–6Al–4V at ambient and elevated temperatures.* Materials Science and Engineering: A, 2003. **355**(1-2): p. 216-230.
33. Nikitin, I., et al., *Mechanical and thermal stability of mechanically induced near-surface nanostructures.* Materials Science and Engineering: A, 2005. **403**(1): p. 318-327.
34. Meyer, D., *Cryogenic deep rolling–An energy based approach for enhanced cold surface hardening.* CIRP annals, 2012. **61**(1): p. 543-546.
35. Meyer, D., E. Brinksmeier, and F. Hoffmann, *Surface hardening by cryogenic deep rolling.* Procedia Engineering, 2011. **19**: p. 258-263.

36. Deutsches Institut für Normung., *DIN 50125:2016-12 Testing of metallic materials - Tensile test pieces*. 2016: Berlin.
37. ASTM International., *ASTM E92-17 Standard Test Methods for Vickers Hardness and Knoop Hardness of Metallic Materials*. 2017, ASTM International: West Conshohocken, PA.
38. ASTM International., *ASTM E384-17 Standard Test Method for Microindentation Hardness of Materials*. 2017, ASTM International: West Conshohocken, PA.
39. British Standards Institution., *BS EN ISO 4287:1998+A1:2009 Geometrical product specification (GPS). Surface texture: Profile method. Terms, definitions and surface texture parameters*. 2000, British Standards Institution.
40. Savaşkan, R.B., *Investigation of Plastic Deformation and Residual Stresses Occured After Deep Rolling Process on Aluminum Alloy 6082 Alloy Using Finite Element Analysis*. 2019, Hacettepe University.
41. Swift, H.W., *Plastic instability under plane stress.* Journal of the Mechanics and Physics of Solids, 1952. **1**(1): p. 1-18.
42. Cockcroft, M.G. and D.J. Latham, *Ductility and the Workability of Metals*. 1968.